AEROSOL RADIATIVE FORCING OVER CENTRAL GREENLAND: ESTIMATES BASED ON FIELD MEASUREMENTS

A Thesis
Presented to
The Academic Faculty

by

Brandon Strellis

In Partial Fulfillment
of the Requirements for the Degree
Master in the
School of Environmental Engineering

Georgia Institute of Technology
August, 2013

AEROSOL RADIATIVE FORCING OVER CENTRAL GREENLAND: ESTIMATES BASED ON FIELD MEASUREMENTS

Approved by:

Dr. Mike Bergin, Advisor

School of Civil and Environmental Engineering

School of Earth and Atmospheric Sciences

Georgia Institute of Technology

Dr. Irina Sokolik

School of Earth and Atmospheric Sciences

Georgia Institute of Technology

Dr. Athanasios Nenes

School of Earth and Atmospheric Sciences

School of Chemical and Biomolecular Engineering

Georgia Institute of Technology

Date Approved: June 6, 2013

ACKNOWLEDGEMENTS

This thesis required the help and guidance of many people. I wish to thank my advisor, Mike Bergin, for his support during my pursuit of this Master's degree, Patrick Wright for his help with spectral albedo measurements and analysis, and Jack Dibb, Florent Domine, Carlo Carmagnola, Hannah James, and Kevin McMahon for their assistance with fieldwork. Thanks to Derek Hagemann, Patrick Sheridan, and John Ogren at NOAA for help with data analysis and understanding the instruments. For radiative modeling, I wish to thank Irina Sokolik, and for help with the CCN analysis, I wish to thank Jack Lin and Aikaterini Bougiatioti. Thanks to the Summit crew and science technicians for all of their help and for being such good company. This project was funded in part by a National Science Foundation Graduate Research Fellowship.

CONTENTS

List of Tables

List of Figures

LIST OF SYMBOLS AND ABBREVIATIONS

σ_{sp}	Particle scattering coefficient
σ_{ap}	Particle absorption coefficient
τ	Aerosol optical depth
ω	Single scattering albedo
$å_{sp}$	Angstrom scattering exponent
$å_{ap}$	Angstrom absorption exponent
R_s	Surface albedo
AOD	Aerosol optical depth
SZA	Solar Zenith Angle
TOA	Top of atmosphere
RFE	Radiative Forcing Efficiency
CCN	Cloud condensation nuclei
DARF	Direct aerosol radiative forcing
DARF TOA	Direct aerosol radiative forcing at the top of the atmosphere

SUMMARY

In light of the significant role that aerosols play in the radiation balance over Greenland and the essential role of the Greenland ice sheet in the Arctic and globally, it is necessary that key measurements of aerosol physical and chemical properties be made in situ so that accurate radiative modeling can be done for the ice sheet. In order to meet this end, measurements of the key aerosol properties including light scattering and backscattering coefficients (σ_{sp} and σ_{bsp}), light absorption coefficient (σ_{ap}), and particle concentration were made at Summit, Greenland, in the summer of 2011. From these quantities, the single scattering albedo (ω) and angstrom scattering and absorption exponents ($å_{sp}$, $å_{ap}$) were calculated. In conjunction with these measurements, aerosol optical depth (AOD or τ) and the spectral surface albedo, R_s, were measured. Additionally, the aerosol chemical composition was characterized through snow and air filter analyses. Taken as a whole, this project allowed for the first ever measurement-based characterization of aerosol radiative forcing over central Greenland. These measurements will serve to validate and refine future attempts to model the Arctic in both regional and global climate models (GCMs). Furthermore, an instrument suite was established as part of the National Oceanic and Atmospheric Administration's Earth Science Research Laboratory Global Monitoring Division (NOAA ESRL GMD) network of monitoring sites which will collect a long-term record of key aerosol properties at Summit for use in future research.

The study yielded measurements of key aerosol properties for the summer of 2011 and, at the time of this writing, the instrument suite at Summit continues to record key

aerosol properties. In summer 2011, the mean value of σ_{sp} was 1.76 ± 1.23 Mm^{-1}; the mean value of σ_{ap} measured by our PSAP was 0.14 ± 0.12 Mm^{-1}, and the mean value of σ_{ap} measured by our CLAP was 0.15 ± 0.13 Mm^{-1}. The mean value of the single scattering albedo calculated with our CLAP was 0.93 ± 0.03. From May 2011 to January 2013, the mean value of σ_{sp} was 1.27 ± 2.08 Mm^{-1}; the mean value of σ_{ap} measured by our PSAP was 0.12 ± 0.14 Mm^{-1}, and the mean value of σ_{ap} measured by our CLAP was 0.09 ± 0.12 Mm^{-1}; the mean value of the single scattering albedo calculated with our CLAP was 0.91 ± 0.07, indicating that the aerosol load over Summit is relatively highly absorbing for a remote, pristine Arctic site.

The study yielded the following conclusions: first, that aerosol loading over Summit shows a clear seasonal trend and is highest in the spring and late summer/fall and lowest in the winter; second, that the clear sky instantaneous direct aerosol radiative forcing at the top of the atmosphere (DARF TOA) has a value of 11.2 ± 4.0 W m^{-2}, which is of much greater magnitude and opposite sign compared to the IPCC estimate of global DARF which has a value of -0.5 (-0.9 to -0.1) W m^{-2}; third, that the radiative forcing efficiency (RFE) of the aerosol over Greenland is very high with a value of 127 ± 28 W m^{-2}; fourth, that variability in surface albedo (R_s) can alter DARF TOA by approximately 0.25 – 1 W m^{-2}; fifth, that variability in single scattering albedo can alter DARF TOA by approximately 5 – 15 W m^{-2}.

CHAPTER 1

INTRODUCTION AND BACKGROUND

Modeling and observational studies indicate that the global climate is warming under the influence of anthropogenic emissions related primarily to fossil fuel combustion. Observations of climate change have established that global mean surface temperature has increased by 0.13 [0.10 to 0.16]°C per decade over the last 50 years (1956 – 2005) [*IPCC*, 2007], snow and ice surfaces in the cryosphere have experienced increased rates of melting [*Mote*, 2007], and global mean sea level has risen at 1.7 ± 0.3 mm per year from 1870 to 2004 [*Church and White*, 2006]. Moreover, these changes have accelerated in the last half of the twentieth century [*IPCC*, 2007]. Climate models have demonstrated that these changes are linked to a warming atmosphere [*Vermeer and Rahmstorf*, 2009]. There have been observations of changes in frequency and duration of extreme weather events and precipitation [*IPCC*, 2007], although there is large uncertainty in predicting the effects of climate change on many weather phenomena such as cyclones [*Knutson et al.*, 2010]. Additionally, the effects of climate change have also been observed in disruptions of or alterations to biological systems on land and in salt- and freshwater. These changes include earlier migration times for birds, shifts in range and distribution of species, and earlier budding of trees due to longer, warmer growing seasons [*IPCC*, 2007].

1.1 A Brief Overview of Climate Change Mechanisms

Chemical components of the atmosphere which significantly influence climate change include greenhouse gases, clouds, and aerosol particles. The greenhouse gases CO_2 and water vapor have the largest overall effect on the radiation balance due to their concentration in the atmosphere and their radiative properties, but water vapor is not generally produced directly by anthropogenic activities [*IPCC*, 2007; *Karl and Trenberth*, 2003]. The anthropogenic input to the atmosphere with the largest influence on the radiation budget is CO_2 [*Lashof and Ahuja*, 1990]. Greenhouse gases heat the atmosphere because they absorb radiation in the infrared wavelengths which the earth emits. Upon absorbing the IR radiation emitted by the earth, CO_2 and other greenhouse gases heat up and in turn reradiate energy, typically in the IR wavelength, both towards the earth and towards space. Increased amounts of CO_2 and other greenhouse gases increase the amount of heat trapped in the earth's atmosphere, thereby causing warming. Figure 1 is a simple representation of how the atmosphere affects the radiation budget. Essentially, the atmosphere absorbs heat radiated from the surface; a larger fraction of that heat is then reradiated back to the surface rather than being emitted to space.

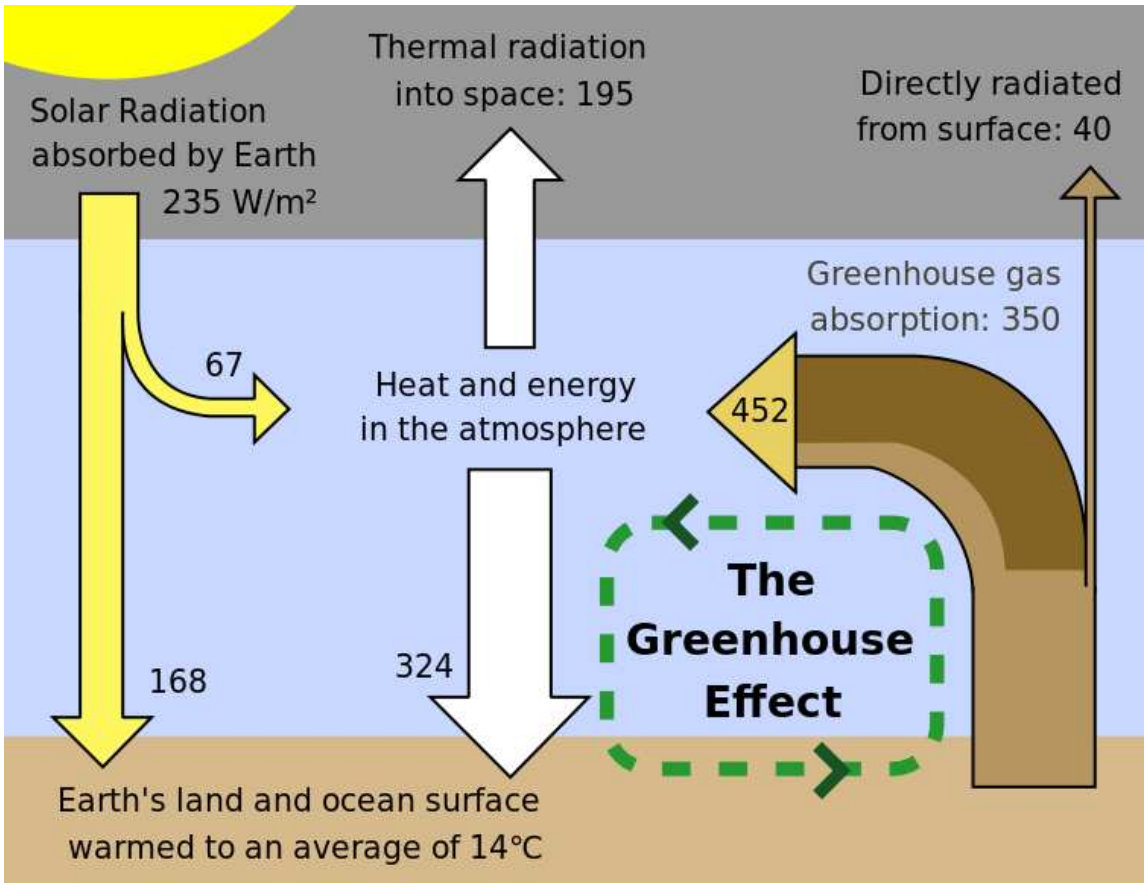

Figure 1: A simplified schematic of the greenhouse effect. Figure created by Robert A. Rohde.

However, the situation is complicated by many other factors such as geochemical cycles and atmospheric dynamics. It has been demonstrated by models that some key processes in the environment such as the carbon cycle [*Cox et al.*, 2000] and the formation of atmospheric water vapor [*Soden et al.*, 2002] are positive feedback loops which will enhance any warming generated by increased levels of CO_2 in the atmosphere. There is, therefore, a risk that global climate will change more rapidly than we can predict in response to anthropogenic forcing.

From 1970 to 2004, CO_2 levels in the atmosphere have increased by 80% [*IPCC*, 2007]. CH_4 and N_2O levels have also increased dramatically in that time. These gases are

sourced primarily from fossil fuel combustion and agriculture. Despite increases in energy efficiency, global population and economic growth have served to increase overall energy consumption and greenhouse gas production to the point that CO_2 and CH_4 are both at levels far beyond any seen in the past 650,000 years of geologic records [*IPCC*, 2007].

The overall effect of these anthropogenic inputs to the atmosphere has been to alter the radiation balance of the earth such that the atmosphere has warmed. The IPCC [*IPCC*, 2007] estimates that the global average net effect of anthropogenic activities since 1750 has led to a radiative forcing of +1.6 (0.6 – 2.4) W m^{-2}. The plus sign is indicative of a warming effect.

1.2 Significance of Aerosols in Climate Change

In addition to greenhouse gases, aerosols are a significant component of the Earth's climate system. Aerosols, or particulate matter, are microscopic particles in the solid or liquid phase which are suspended in a gas. These particles range in size from a few nanometers to hundreds of microns. The size of the particle has a significant effect on its chemistry and fate in transport [*Hinds*, 1982]. Generally, small aerosols can persist for longer periods in the atmosphere and can be transported over longer distances than large particles, but this depends not just on particle size but on chemical and photochemical reactivity [*Seinfeld*, 1998]. Larger particles with higher settling velocities tend to deposit to the surface more quickly. Besides particle diameter, aerosol absorption and scattering are functions of the shape of the aerosols, the relative humidity, and the wavelength of incident light [*Yu et al.*]. Due to the wide variability in size, composition, and reactivity of aerosols, they tend to be heterogeneously distributed around the globe.

By comparison, CO_2 has a lifetime of approximately ten years in the atmosphere before it is absorbed by the oceans [*Revelle and Suess*, 1957]. As a result, CO_2 tends to be more homogeneously distributed in the atmosphere over space and time than are aerosols. This means that models can more easily predict the radiative forcing by CO_2 than the radiative forcing by aerosols.

Anthropogenic aerosol inputs to the atmosphere include black carbon (BC, also known as elemental carbon, EC), brown carbon, organic carbon (OC), sulfates, nitrate, ammonium, and dust [*IPCC*, 2007]. Many of these aerosols are produced primarily or secondarily by combustion of fossil fuels for transportation, power generation, biomass burning, and residential cooking and heating.

Light scattering aerosols and light absorbing aerosols have distinct effects. "Scattering" and "absorbing" refer to their interactions with solar radiation. Scattering aerosols have a net negative direct RF at the TOA due to their scattering light back to space regardless of the surface over which they lie; absorbing aerosols have a net negative direct RF at the TOA over dark surfaces such as forest and oceans, but a net positive TOA RF over bright surfaces such as snow and desert[*IPCC*, 2007]. This is because reflective surfaces will lead to multiple opportunities for absorption of solar irradiance by the aerosol [*Chylek and Wong*, 1995; *Haywood and Shine*, 1995]. Both scattering and absorbing aerosols reduce the amount of solar irradiance that reaches the surface, thereby causing a negative RF at the surface [*IPCC*, 2007]. Generally, the interactions with solar radiation cause a greater RF than interactions with terrestrial radiation because the particles must be large enough, in high enough concentrations, and

at certain levels of the atmosphere to interact significantly with longwave radiation, which is seldom the case [*Goodale and Mansfield*, 1987].

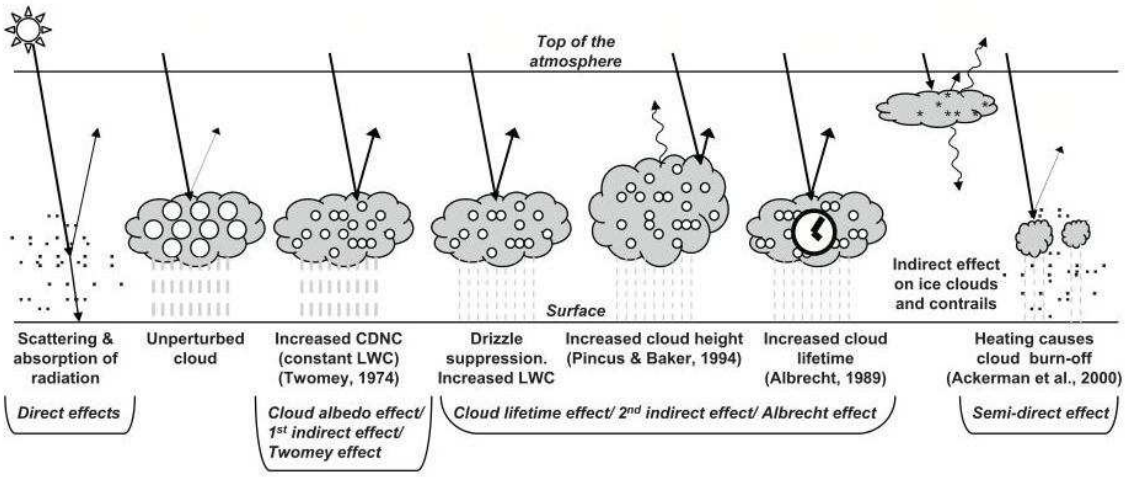

Figure 2: Aerosol effects in the atmosphere. The black dots represent aerosols, the open white circles cloud droplets, the vertical grey dashes precipitation, straight lines solar radiation, and wavy lines terrestrial (longwave) radiation. LWC refers to liquid water content. CDNC refers to cloud droplet number concentration. Figure from the Intergovernmental Panel on Climate Change Fourth Assessment Report.

There are at least four ways in which aerosols influence the climate, as illustrated by Figure 2. The first effect is the direct aerosol effect, which is the absorption or scattering of light by the aerosols themselves [*McCormick and Ludwig*, 1967]. It should be noted that some aerosols, such as sulfate, scatter solar radiation but absorb terrestrial radiation. Additionally, aerosols exert an indirect effect in which they act as cloud condensation nuclei, thereby affecting the properties of clouds including area and persistence of cloud cover [*Twomey*, 1977] as well as precipitation. Unperturbed clouds contain larger cloud drops as only natural aerosols are available as cloud condensation

nuclei (CCN), while the perturbed cloud contains a greater number of smaller cloud drops as both natural and anthropogenic aerosols are available as CCN. The indirect effect is itself split into two effects: the cloud albedo effect due to alteration of the cloud radiative properties, e.g., reflectivity and particle size, and the cloud lifetime effect due to the aerosols extending the duration of cloud cover [*Haywood and Boucher*, 2000]. Finally, as a result of the direct effect, aerosols alter the temperature structure of the atmosphere by heating the air and reducing the relative humidity, thereby decreasing cloud formation; this is termed the semi-direct effect [*Hansen et al.*, 1997b]. All of these effects have significance for climate change.

It is thought that the aerosol direct effect has a global average cooling effect at the surface and TOA [*Bellouin et al.*, 2005]. The IPCC estimated that anthropogenic aerosols have a net global direct radiative forcing of -0.5 (-0.9 to -0.1) W m^{-2} at the TOA [*IPCC*, 2007]. In other words, past models have indicated that the cooling effect of light-scattering aerosols outweighed the warming effect of light-absorbing aerosols at the TOA. However, most of these past results were based on models which did not include brown carbon, the absorptive component of organic aerosols. As a result, organic aerosols were treated as primarily light-scattering. Recent studies indicate that when the absorption of solar radiation by brown carbon is taken into account, global net direct RF by organic aerosols is approximately zero – that is, it neither warms nor cools the planet – while BC may have a warming effect of up to +0.65 (0.5 – 0.8) W m^{-2} at the TOA [*Chung et al.*, 2012]. One study showed that the surface direct RF will be approximately equal to the TOA RF for scattering aerosols, but for absorbing aerosols the surface RF may be several times higher than the TOA direct RF [*Ramanathan et al.*, 2001]. This

suggests that a small amount of absorbing aerosols over a highly reflective surface could cause a large surface warming, which has implications for high-albedo locations such as the Arctic. The aerosol indirect effect also has a global average cooling effect. The cloud albedo effect is thought to make clouds more reflective because submicron aerosols acting as cloud condensation nuclei bias the cloud water droplet formation towards smaller droplets, increasing the number of cloud water droplets per unit volume, thereby increasing the number of particles with which radiation can interact [*Twomey et al.*, 1984]. This leads to more scattering of solar radiation back to space due to the increased optical thickness of the cloud. The cloud lifetime effect is also linked to the decreased water droplet size and increased water droplet concentration because these changes to the structure of the cloud lead to reduced precipitation efficiency, which extends the lifetime of the cloud [*Albrecht*, 1989]. The result is longer-lived clouds which are more reflective to solar radiation. Contrarily, the aerosol semi-direct effect leads to decreased cloud formation by heating the atmosphere and reducing the relative humidity. This exerts a warming effect. Modeling studies indicate that this semi-direct effect could be of a similar magnitude to the direct radiative forcing [*Johnson et al.*, 2004]. This is particularly important in the troposphere where anthropogenic aerosol loadings are highest [*Hansen et al.*, 1997a]. It is estimated that anthropogenic aerosols have a net global indirect cloud albedo forcing of -0.1 (-1.8 to -0.3) W m^{-2} [*IPCC*, 2007]. This estimate does not include the semi-direct effect since at the time of the IPCC report it was not included in many model simulations.

It should be noted that there are still very large shortcomings in our understanding of aerosols and in our ability to model them accurately. These include uncertainties in

emissions inventories, incomplete characterization of the many different types of aerosols which have a radiative effect, and lack of understanding of aerosol-cloud interactions. For example, in many past studies the absorption of solar radiation by organic carbon aerosols was considered negligible; organic aerosols were treated as primarily light-scattering. It is now understood that organic aerosols have a large light-absorbing fraction. On another front, aerosol-cloud interactions are being studied with great interest in order to help improve model predictions of changes to cloud behavior. In other words, while aerosol science is of huge significance to climate change, it is a field in which many contributions remain to be made.

1.3 Significance of Aerosols in the Arctic

Models and observations have shown that the Arctic is particularly susceptible to climate change [*Krupnik and Jolly*, 2002; *Washington and Meehl*, 1989]. Since the 1970s, the temperature at the top of the permafrost layer has been observed to have generally increased [*Romanovsky et al.*, 2010]. In Greenland, more glacial lakes are forming as the result of surface melting, and glacial run-off is occurring in larger volumes than have been observed in the recent past [*Abdalati and Steffen*, 2001; *Hanna et al.*, 2008]. It is therefore clear that the factors which influence climate change in the Arctic must be well understood.

Aerosols play a significant role in Arctic climate through RF effects in the air and snow. Because of the long, dark Arctic winter, a relatively low amount of solar energy is available annually for absorption. As a result, changes by aerosols to the radiative flux of the Arctic have a significant impact [*Valero et al.*, 1989].

Examples of aerosols which are of significance in the Arctic include sulfate, black carbon, organic carbon (which is converted into brown carbon), and dust. Black carbon and brown carbon aerosols are of particular interest because they are very efficient absorbers of solar radiation. This property, in combination with the highly reflective ice and snow surfaces of the Arctic, creates a circumstance in which aerosols can have a warming effect throughout the surface-atmosphere column rather than a warming effect in the atmosphere and a cooling effect at the surface. These aerosols act as cloud condensation nuclei as well as ice nuclei.

Black and brown carbon are the primary light-absorbing aerosol species besides dust. Black carbon is thought to be an aerosol of particular importance to climate change because it is a highly effective absorber of solar and terrestrial radiation, with some estimates placing its total radiative forcing second only to that of CO_2 [*Jacobson*, 2001]. Additionally, it can deposit to snow and ice surfaces and reduce the surface albedo [*Warren and Wiscombe*, 1980]. Brown carbon is the absorbing component of organic carbon aerosols, and it, too, is a significant absorber of radiation, with recent modeling results indicating a global forcing of +0.25 W m^{-2} attributable to brown carbon [*Feng et al.*, 2013]. Globally, black and brown carbon have a warming effect at the top of the atmosphere and a cooling effect at the surface because they absorb solar radiation at the top of the atmosphere, which heats the atmosphere while preventing the solar radiation from reaching the earth's surface. The decrease in solar irradiance at the surface causes the cooling effect.

The Arctic tends to have a seasonal pattern of aerosol loading in which the concentration of aerosols is increased during the winter and spring due to long-range

transportation of anthropogenic aerosols as well as slow removal processes [*Sirois and Barrie,* 1999]. This phenomenon is known as Arctic Haze, and it persists because removal processes for aerosols consist of scavenging by precipitation and deposition to surfaces; precipitation is normally low during the Arctic winter [*Shaw,* 1981] and is decreased in part by aerosol interactions with clouds, while deposition to surfaces is inhibited in the Arctic by stable temperature inversions which prevent atmospheric mixing and, in the process, deposition of aerosols to the surface. Because of the slow removal processes, aerosols tend to have much longer lifetimes in the Arctic than they do elsewhere.

Anthropogenic aerosols in the Arctic are generally sourced from the northern mid- and high latitudes due to meteorological patterns such as the North Atlantic Oscillation [*Eckhardt et al.,* 2003]. Major sources for Arctic aerosols include industry in Europe, North America, and Asia, and forest fires and biomass burning in Canada and Siberia [*Frossard et al.,* 2011; *Warneke et al.,* 2010]. Recent observations of aerosol transport to the Arctic from mid-latitudes has shown that increasing temperatures in the Arctic may lead to more facile transport of aerosols from polluted lower latitudes, resulting in enhanced warming [*Quinn et al.,* 2008].

The aerosol direct effect over the Arctic is affected by the surface albedo of the land surface, the type of aerosol present, and the season. In the late spring, summer and early fall, when the Arctic is exposed to solar irradiance, solar light-absorbing aerosols intercept solar radiation and heat up the atmosphere, thereby cooling the surface by preventing solar irradiance from reaching it. Solar light-scattering aerosols also cool the surface. It is thought that the net direct effect of aerosols in the Arctic is a warming effect

in the atmosphere and a cooling effect at the surface [*Emery*, 1990]. The RF is particularly pronounced during the winter and spring when concentrations of anthropogenic aerosols are higher. Additionally, the absorption of solar radiation by aerosols is enhanced by the high solar reflectivity of the snow and ice surfaces in the Arctic, resulting in an even greater warming effect. The reflectivity of Arctic surfaces is so high that aerosols with a single scattering albedo of up to 0.98 can still have a warming effect on the surface-atmosphere column [*Pueschel and Kinne*, 1995]. The direct radiative effect of the heavy springtime aerosol loading in the Arctic has been estimated at 2.5 W m^{-2} at TOA and -0.93 W m^{-2} at the surface [*Quinn et al.*, 2007]. This estimate does not, however, indicate what the annual direct forcing by aerosols might be.

The aerosol indirect effect over the Arctic causes a net warming effect at the surface during the Arctic winter due to the emission of longwave infrared radiation. The magnitude of this effect may be as great as 3 W m^{-2} in the winter [*Garrett et al.*, 2002]. If the aerosols act as cloud condensation nuclei and form clouds, their longwave radiative effect is enhanced [*Quinn et al.*, 2007]. This is due to a combination of the indirect effects discussed previously. The cloud albedo effect leads to higher solar albedo but also higher infrared emissivity of clouds, resulting in more infrared radiation warming the land surface [*Garrett et al.*, 2002], while the cloud lifetime effect leads to more enduring clouds which similarly contribute more infrared radiation to warming the surface [*Hobbs and Rangno*, 1998]. Although our understanding of the aerosol indirect effects in the Arctic is still developing, modeling studies indicate that the indirect effect has a net annual warming influence on the Arctic surface [*Shindell and Faluvegi*, 2009].

Recent studies indicate that climate models may underestimate the effect of aerosol radiative forcing by a factor of 2-5, especially in remote regions [*Feng et al.*, 2013]. However, it is difficult to compare models to observations over much of the Arctic due to the lack of areal and temporal coverage in measurements.

1.4 Significance of Surface Albedo in Cryosphere

Surface albedo is of crucial importance to aerosol radiative forcing in the Arctic because the highly reflective surface increases solar light absorption by atmospheric aerosols. Additionally, dark particles such as black carbon can deposit to snow surfaces and reduce the albedo. This latter effect may cause a warming at the surface in the winter of 0.1 W m^{-2} and a larger warming of 1.7 W m^{-2} in the spring [*Wang et al.*, 2011]. This warming of the surface and lower atmosphere can lead to increased snow and ice melt [*Quinn et al.*, 2008]. It should be noted that while deposition of dark particles to snow and ice surfaces may be a significant component of some regional Arctic processes, it does not appear to be a significant factor over central Greenland due to extremely low concentrations of black carbon in surface snow [*Hagler et al.*, 2007].

1.5 Significance of the Greenland ice sheet

One area in which very few measurements of key aerosol properties has been made is the Greenland ice sheet. The Greenland ice sheet is a geologic feature of critical importance to the Arctic and the globe. It covers approximately 660,000 square miles and contains enough water to dramatically increase global sea level if it were to melt. Because of the vast extent and high surface albedo of the Greenland ice sheet, it is a crucial factor in radiative processes in the Arctic. The Greenland ice sheet is also unique

in that much of the ice sheet is at high altitude, which leads to altered aerosol loadings and meteorology from much of the rest of the Arctic. Despite the obvious importance of the ice sheet in regional and global climate change, measurements of key climatic properties have not been made extensively on the ice sheet due to its vast size and harsh conditions.

1.6 Overview of this Study

Measurements of key aerosol properties including light scattering and backscattering coefficients (σ_{sp} and σ_{bsp}), light absorption coefficient (σ_{sp}), and particle concentration were made at Summit, Greenland, in the summer of 2011. Aerosol optical depth (AOD or τ) was measured as conditions allowed and the spectral surface albedo, R_s, was measured on a daily basis. Additionally, the aerosol chemical composition was characterized through snow and air filter analyses. These measurements were used to create a data set for use in radiative modeling of the ice sheet. This constitutes, to our knowledge, the first quantification of radiative forcing over the Greenland ice sheet based on in-situ measurements.

CHAPTER 2

Methodology

2.1 Location

The measurement campaign for this study was conducted at Summit, Greenland, which is a National Science Foundation research base located at 72°35'46.4"N, 38°25'19.1"W. The base is 10,350 ft above sea level and in the middle of the Greenland ice sheet, far removed from any aerosol sources besides the camp generator and heavy machinery used to maintain the runway. As such, it is a site representative of the majority of the Greenland ice sheet.

Summit Camp has a designated clean sampling sector approximately one mile south of the main camp. It is the policy of the camp to limit emissions from the diesel generator and heavy machinery during periods of north winds when the pollution would be carried over the clean air sector. There are several small sampling buildings in this sector, one of which housed our continuous aerosol sampling instrumentation.

Careful records are kept at Summit to ensure that measurement campaigns do not overlap with areas contaminated by prior researchers.

2.2 Aerosol Measurements

Aerosols were measured via three separate methods during the course of this study: by instruments sampling aerosols from the air in real-time, by handheld sun

photometers which took instantaneous aerosol measurements, and by air and snow filters which were collected over multiday periods and analyzed after the conclusion of fieldwork.

2.2.1 Real-time Aerosol Sampling Instruments

A suite of real-time aerosol sampling instruments was established at Summit upon our arrival in early May of 2011. The instruments were a Radiance Research Particle Soot Absorption Photometer (PSAP), a Continuous Light Absorption Photometer (CLAP) designed and built by the National Oceanic and Atmospheric Administration, a Droplet Measurement Technologies Cloud Condensation Nuclei (CCN) Counter, a TSI Nephelometer, and a Lasair Optical Particle Counter (OPC). The PSAP, CLAP, nephelometer, and OPC were installed and operating on May 6, 2011. The CCN counter was installed and operating on June 15, 2011. The CCN counter and the OPC were uninstalled on July 18, 2011, while the PSAP, CLAP, and nephelometer were left in place as part of a long-term NOAA sampling effort.

The instrument suite was housed in the Temporary Atmospheric Weather Observatory (TAWO) in the clean air sector. TAWO is a one-story building that is elevated approximately ten feet above the snow surface. The sampling line was attached to the roof of TAWO, approximately twenty feet off of the ground. The intake of the sampling line was protected from debris by a 16.7 lpm $PM_{2.5}$ cyclone (URG Corp., #URG-2000-30EH) operated at approximately 10 lpm. From the cyclone, the line ran through non-polar tubing to a flow splitter, and from the flow splitter out to each instrument.

2.2.1.1 Instrument Sampling Techniques

The PSAP and CLAP measure the absorption coefficient of aerosols by pulling a flow of air through a quartz filter and measuring the change in transmittance as particles deposit onto the filter. The PSAP and CLAP recorded minute-averaged data. The calculation of σ_{ap} is according to the Beer-Lambert Law. The PSAP measures σ_{ap} at λ = 565 nm, while the CLAP measures σ_{ap} at λ = 467, 528, and 652 nm. The PSAP and CLAP have the Bond correction [*Bond et al.*, 1999] applied. Without the Bond correction, error in the PSAP measurements is on the order of 20 – 30%. After the Bond correction is applied, total instrument uncertainty is estimated at 15% for a one-minute averaging time and typical atmospheric levels of absorption [*Bond et al.*, 1999]. According to one study, noise for the 1-λ PSAP for a 60 s sampling interval is, on average, 0.05 Mm^{-1} [*Muller et al.*, 2011]. The uncertainty in PSAP measurements of the absorption coefficient increases as the single scattering albedo increases [*Muller et al.*, 2011].

The nephelometer measures the scattering and backscattering coefficients (σ_{sp} and σ_{bsp}) of aerosols by measuring the total light scattered in a special chamber and then subtracting the light scattering contributions of the chamber walls, the gas, and electronic noise. The nephelometer measures σ_{sp} and σ_{bsp} at λ = 450, 550, and 700 nm.

The OPC measures particle concentration (cm^{-3}) in a number of size bins by measuring the light scattered by each particle. The size bins are 0.1 – 0.2 µm, 0.2 – 0.3 µm, 0.3 – 0.4 µm, 0.4 – 0.5 µm, 0.5 – 0.7 µm, 0.7 –1.0 µm, and 1.0 – 2.0 µm. The CCN counter measures aerosol particles which can act as cloud condensation nuclei by pulling the particles through a chamber supersaturated with water vapor and then counting the

particles that have formed droplets with an OPC. The supersaturation can be varied between 0.07 – 3.0%. The OPC within the CCN counter detects particles greater than 0.3 µm [*Roberts and Nenes*, 2005].

2.2.1.2 Quality Analysis Procedures for Real-time Instrument Data

Real-time instrument data was collected by a NOAA software program (LiveCPD). Another program (AER_VM) allowed for graphical and numerical quality analysis of the data. LiveCPD calculates the light scattering and absorption coefficient data at 450, 550, and 700 nm. Because the real-time instruments sampled air continuously, there were occasional contamination events from camp or from passing air traffic. These events could be identified by very large spikes in the aerosol parameters which occurred over very short intervals, usually in north winds. This data was flagged as contaminated and removed from our analytical data set. Additionally, there were occasional flow disruptions or instrument irregularities which could be identified by abrupt and unrealistic changes in the flow or in aerosol characteristics. This data was flagged as invalid and also removed from our analytical data set.

2.2.2 Instantaneous Aerosol Measurements

AOD, total column water vapor, and total column ozone were measured using a Solar Light Instruments Sun Photometer and Ozonemeter, respectively. The sun photometer is a handheld instrument which the user points at the sun. Once the detector is aligned with the sun, photodiodes measure the incoming solar irradiance at five different wavelengths. From these measurements, AOD can be calculated using the

Beer-Lambert Law. These measurements were taken under clear-sky conditions with no visible ice crystals in the air and a clear line of sight to the sun. Three measurements were taken simultaneously in each instance so that any anomalous readings could be identified. The procedure used for the sun photometers was similar to the procedure used in studies in Atlanta [*Carrico et al.*, 2003] and Beijing [*Xu et al.*, 2003].

2.2.2.1 Quality Analysis Procedures for Instantaneous Aerosol Measurements

Although every effort was made to only take AOD measurements under clear-sky conditions, additional quality analysis was performed in order to ensure that the measurements were not contaminated by ice crystals in the atmosphere. First, each set of three measurements was checked for consistency. Because the measurements were taken seconds apart, any measurement which deviated greatly from the other two measurements in its set was discarded. These erroneous measurements may have been due to failure by the operator to target the sun accurately while taking the measurement. After this initial screening of the data, the angstrom exponent ($å_{AOD}$) of each measurement was calculated. The data were divided into three quality regimes: $å_{AOD} \leq 0.5$, $0.5 \leq å_{AOD} \leq 1.0$, and $å_{AOD} \geq 1.0$. The highest quality data were those measurements with $å_{AOD} \geq 1.0$ because ice crystals and other large particles tend to drive the $å_{AOD}$ below one [*Schuster et al.*, 2006].

2.2.3 Aerosol Filter Sampling

Air and snow samples were analyzed to determine aerosol chemical composition. These samples were analyzed for elemental carbon (EC), organic carbon (OC), elements, and ions.

2.2.3.1 Air Sampling

Three parallel sampling lines were established on the roof of TAWO. One line sampled ions, one elements, and one ECOC. The intake of each sampling line was protected from debris and ice crystals by a 16.7 lpm $PM_{2.5}$ cyclone (URG Corp., #URG-2000-30EH). The ion line was operated at 25 lpm, the element line at 25 lpm, and the ECOC line at 19 lpm. The flow rate in each line was governed by a critical orifice. A wind-vane constantly monitored the wind direction and speed and shut off the pump if the wind was coming from camp or if the wind was stagnant in order to prevent the filters from sampling contaminated air.

ECOC was captured on a quartz filter (Pall Corp. #2500 QAT-UP, 25 mm), ions on 1µm Fluoropore filter, and elements on a 47 mm Teflon filter. The ECOC filters were prepared by being baked in a 500°F oven for five hours before being wrapped in pre-baked foil and placed in a sealed and Teflon-taped petri dish. This was done in order to ensure that the filters were completely free of ECOC up to the moment that they were installed in the sampling system in Greenland. Ion filters were used straight out of the Fluoropore package. Element filters were prewashed with acid and Milli-Q water and stored in polystyrene petri dishes which had been soaked in acid and washed with Milli-Q water [*Lough et al.*, 2004].

Samples were collected for 3-6 days depending on weather conditions. Filters were changed under a fume hood inside one of the buildings using pre-baked tweezers. All possible precautions were taken to avoid contaminating the filters during their placement in the filter holder or during their removal. After the sample-laden filters were removed from the filter holders, they were returned to the petri dish from which they

came, resealed with Teflon tape, and stored in a snow cave at approximately -20 °F to await shipment back to their respective analytical institutions. For shipment, the filters were packed in ice and surrounded with ice packs to ensure that they stayed as cold as possible in transit. The procedures used were the same as those used by Hagler et al [*Hagler et al.*, 2007; *Hagler et al.*, 2007b].

2.2.3.2 Snow Sampling

From May 15, 2011, to July 19, 2011, samples were collected daily from surface snow in the clean air sector of Summit camp. Each day at approximately 1030 local time (1230 GMT) a new, virgin site was sampled. ECOC and ion samples were collected daily, while element samples were generally collected every third day. Samples were collected facing into the wind so as to avoid debris from the sampler falling onto the snow.

Element and ion samples were scraped into pre-cleaned bottles, the contents of which were kept frozen from the time of collection until the time of analysis. Ion snow samples were collected with a pre-cleaned Lexan scraper and pre-cleaned polyethylene funnel [*Dibb et al.*, 2007]. The ion snow samples were taken, to the best of our ability, from the three uppermost layers of snow. Typically, the first layer was a few millimeters of newly deposited snow or rime, the second layer was 0.5 – 2 cm of powder, and the third layer was 0.5 – 2 cm of crust, but there was greater and lesser variability from day to day.

ECOC samples were collected by scraping a jar across the top three inches of the snowpack. Prior to the trip, the ECOC sampling jars had been cleaned extensively with

isopropyl alcohol and deionized water to remove any traces of ECOC. Ten one-liter jars of snow were collected for each ECOC sample. This snow was then melted, and the water was pulled through a quartz filter. As a result, the OC remaining on the filter was water insoluble, as the water soluble OC passed through the filter. Analysis of these filters was therefore for EC and water insoluble organic carbon (WIOC). The wet filter was then dried for 12-24 hours under a fume hood before being repacked into a clean aluminum foil pouch within a petri dish, sealed, and put in the camp freezer.

2.2.3.3 Filter Analysis

Each type of filter was analyzed at a different institution. ECOC filters were analyzed at Georgia Institute of Technology, ion filters were analyzed at University of New Hampshire, and element filters were analyzed at University of Wisconsin at Madison.

ECOC filters were analyzed by a Sunset Laboratory Carbon Aerosol Instrument Model 4F. This instrument works by conducting two stepped-temperature oxidations of OC and EC, respectively, and measuring the subsequent products with a flame ionization detector.

The elements were analyzed by inductively coupled plasma mass spectrometry (ICP-MS). The snow samples were melted and pre-digested with 2% nitric acid in-bottle. The baseline was established with a minimum instrument blank. The air filters were pre-digested and diluted one to one with Milli Q water [*Lough et al.*, 2004].

The ions were analyzed by ion chromatography (IC). Prior to analysis, filters were wetted with 100 µl chromatography-grade MeOH and then extracted with 20 ml of Milli

Q water. Snow was melted in-bottle prior to IC. Mean blank corrections were applied to the filters, but this was not done for the snow samples because none of the snow samples showed significant levels of ions. Elevated levels of Na, Cl, and K were used as indicators of contamination. Additionally, snow samples were checked for ratios of cations to anions, Cl to Na, and NH_4 to SO_4 [*Dibb*, 2013].

2.3 Spectral Albedo Measurements

From May 16, 2011, to July 19, 2011, **s**pectral albedo was measured on a daily basis at approximately 1100 local time (1300 GMT) at four fixed sites roughly 5 m apart in the clean air sector. The four sites were marked by bamboo stakes and were undisturbed throughout the campaign. The distance between the stakes was chosen because it was the approximate distance for macroscale changes that could be observed in the snow surface. In addition to the four fixed sites, a fifth spectral albedo measurement was taken each day at a roving site, which site was then used for characterization of snow specific surface and density.

The spectral albedo was measured with an Analytical Spectral Devices Fieldspec Pro spectroradiometer (2001 model) with an ASD Remote Cosine Receptor foreoptic. The spectroradiometer operates by projecting light that enters the foreoptic onto a holographic diffraction grating which enables separation and measurement of the light across three detectors. This instrument measured light in the wavelength range of 350 – 2200 nm. The albedo was defined as the ratio of the upwelling to downwelling irradiance.

The foreoptic was mounted on an aluminum arm 109 cm in length which the user oriented alternately towards the sun and towards the earth. The aluminum arm was held out parallel to the ground and perpendicular to the user's body while a leveling bubble on

the aluminum arm was used to determine the precision and steadiness of the stance. When the leveling bubble indicated that the arm was parallel and steady, a measurement was taken. This technique was chosen over the use of a tripod because it enabled much more rapid measurements without a significant sacrifice of precision. It was necessary to make rapid measurements as the computer would shut down quickly due to the extremely low temperatures at Summit. Four measurements were made at each stake in order to identify operator error in the measurements.

The approximate height for the measurement was 90 cm off of the ground, although this is a generalization as multiple users of different height were responsible for taking the measurements. At this height, the foreoptic has a 2 m field of view radius for 90% of the signal. Although the user stood down-sun when taking albedo measurements so that his shadow did not fall across the measurement space, the user's body still interfered with the signal and needed to be corrected for. Additionally, the shadow of the aluminum arm itself needed to be corrected for. These correction factors are discussed in greater detail in Wright, 2012. A cosine correction factor was not applied to the albedo measurements, although this could potentially increase the spectral albedo curves by approximately 1%.

Each set of four albedo measurements was screened for precision, and obvious outliers were thrown out. Additionally, there were two levels of quality analysis. The first level screened for instrumental error, evidenced by the misalignment of data between two adjacent light detectors. The second level of quality analysis required combing the actual albedo profiles and removing data that had values greater than one in the ultraviolet/visible spectrum or that displayed a known instrument error, of which there

are several. Most of the bad data was the result of changing cloud conditions during the course of the measurement series.

Extensive information regarding the methods and results of the spectral albedo measurements can be found in the literature [*Carmagnola et al.*, 2012; *Wright*, 2012].

2.3 Radiative Modeling

The program used for the radiative modeling was SBDART (Santa Barbara DISORT Atmospheric Radiative Transfer). This is a one-dimensional radiative transfer modeling program composed of physically-based models developed over the past few decades by atmospheric science researchers. Five key areas of the model are clouds, atmospheric gas absorption and scattering, aerosol absorption and scattering, extraterrestrial radiation spectra, and surface type. SBDART has been used extensively by the scientific community for radiative transfer modeling [*Xi and Sokolik*, 2012; *Young et al.*, 2012].

Our modeling used measured aerosol properties as the inputs wherever possible. Inputs to the model included daily averaged AOD, spectral surface albedo from 350-2200 nm, altitude-resolved water vapor profile, surface pressure, daily averaged single scattering albedo at three wavelengths, and total column ozone. All model runs were done under clear sky conditions as we did not have comprehensive cloud fraction data. Twenty two days were modeled, with each day having a unique spectral albedo and aerosol properties. Only those days for which all of the necessary data was available were modeled. The solar zenith angle was held constant at 50.9° to represent a high-sun condition coinciding approximately with the measurement of solar spectral albedo.

Clouds were not included in the modeling study, but it was estimated that cloud fraction for the season was 0.56 based on readings by a ceilometer at Summit. The ceilometer detects liquid water but not ice clouds, and it also does not detect clouds more than 6-7 km above the instrument. For these reasons, the estimate of cloud fraction above does not include ice clouds or high altitude clouds, and it is therefore probably 10-20% low [*Matt Shupe, personal communication*, 2012].

CHAPTER 3

Results and Discussion

3.1 ECOC, Ions, and Elements Measurements

3.1.1 Air Measurements

Air filter measurements of ECOC, ions, and elements were at or approaching analytical instrument detection limits due to prevailing north winds in the summer of 2011 at Summit which reduced the exposure time of the filters below what was needed for meaningful results. As a result, the air filter measurements have been excluded from this thesis.

3.1.2 Snow Measurements

The results in this section are for surface snow measured at Summit during the summer of 2011, as further snow and air sampling was not conducted past the 2011 field season.

Figure 3 shows measured EC concentrations (ng EC g^{-1} snow). Each marker represents a daily average EC concentration. The error bars represent the standard deviation of each set of measurements. EC concentrations were between 0.01 – 5.12 ng g^{-1} with a mean of 0.39 ng g^{-1}. These results agree well with measurements made in the summer of 2006 [*Hagler et al.*, 2007] that found EC of 0.1 – 1.5 ng g^{-1}, but they are slightly lower on average than measurements made in 1988 – 1989 and 1989 – 1990 from

Greenland ice cores drilled at Summit which found EC of 1 – 4 ng g^{-1} and 1.4 – 2.7 ng g^{-1}, respectively [*Cachier and Pertuisot*, 1994; *Chýlek et al.*, 1995]. However, industrial emissions from Europe and North America have declined since that time, which may be reflected by the lower EC concentrations. It is also possible that the differences in values are due to differences in measurement and analysis techniques.

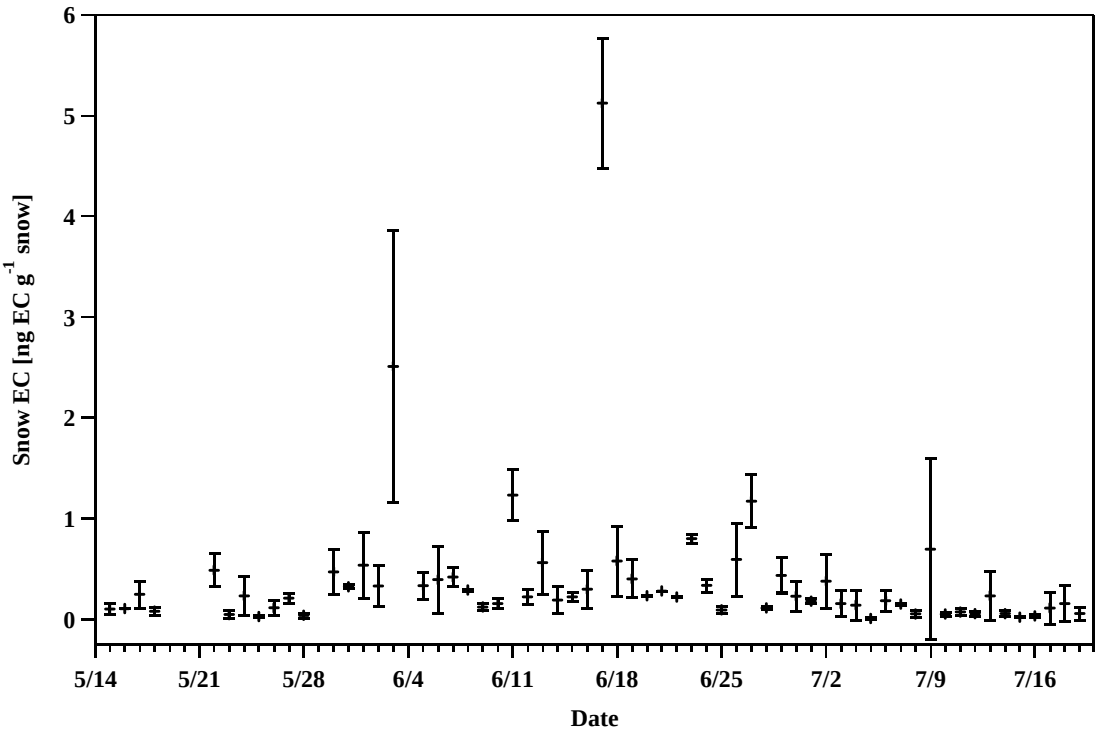

Figure 3: EC concentrations measured in snow.

Figure 4 shows WIOC concentrations measured in snow. Each marker represents a daily average WIOC concentration. The error bars represent the standard deviation of each set of measurements. WIOC concentrations were between 3.2 – 26.5 ng g^{-1} with a mean of 8.5 ng g^{-1}. These results agree well with measurements made in the summer of 2006 at Summit [*Hagler et al.*, 2007] that found WIOC of 5 – 35 ng g^{-1}.

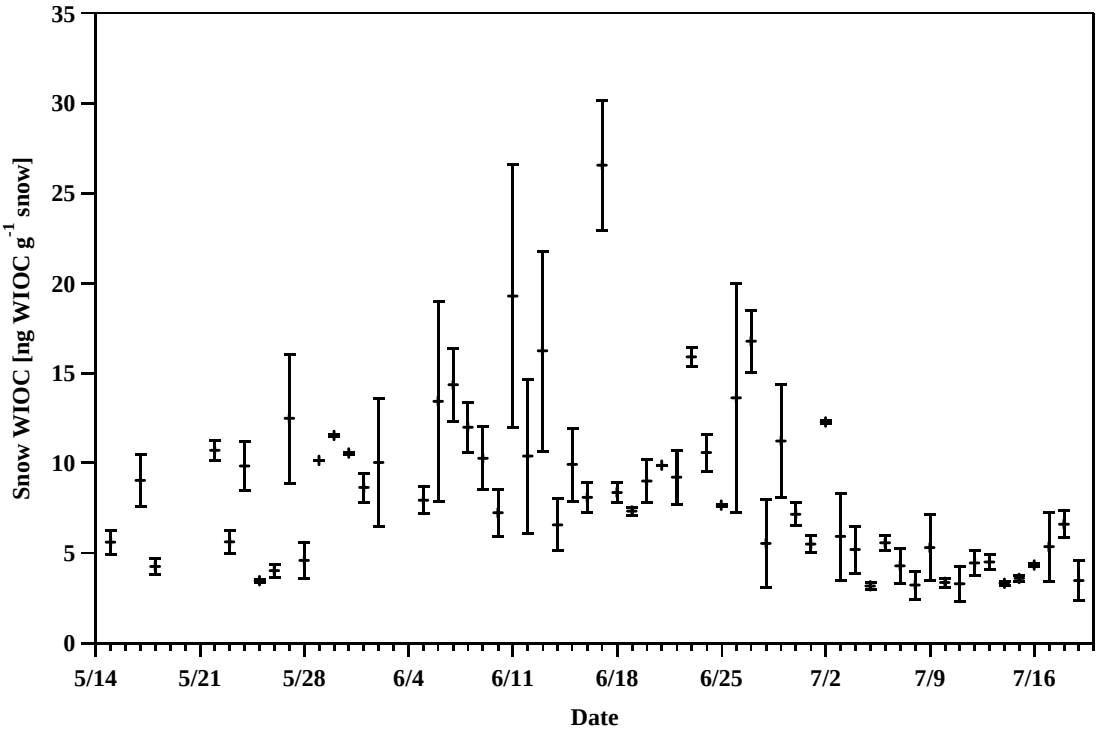

Figure 4: WIOC concentrations measured in snow.

Figures 5 – 10 show ion concentrations in snow. As ions were sampled in three distinct layers, the layers are presented separately here. However, there seems to be no uniform pattern between the layers for all of the ions. The ion measurements are compared to measurements made at Summit during May and June of 1997 and May, June, and July of 2001 [*Dibb et al.*, 2007].

Figure 5 shows Ca^{2+} concentrations measured in snow. Values are between 1 – 96 ng $g^{-1}$with a mean of 15.7 ng g^{-1}. This agrees well with the Dibb campaign measurements which had a mean of 12.9 ± 8.6 ng g^{-1}. There appears to be a slight decrease in Ca^{2+} concentrations starting in the middle of July.

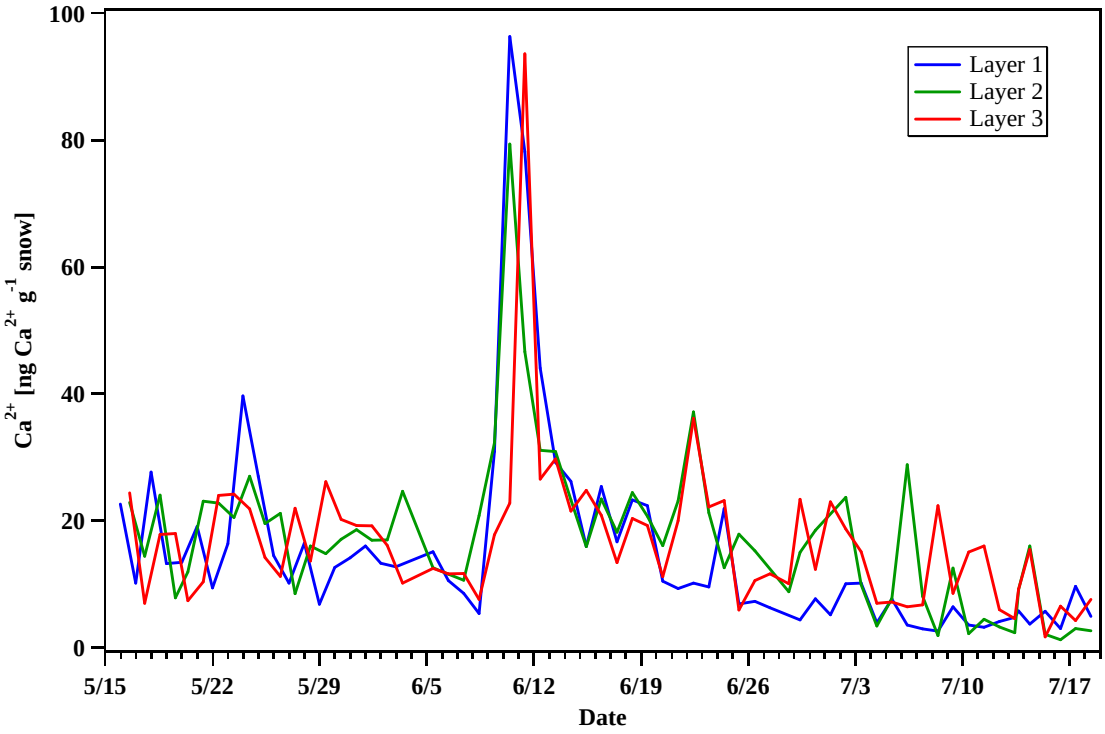

Figure 5: Ca^{2+} concentrations in snow. Typically, the first layer was a few millimeters of newly deposited snow or rime, the second layer was 0.5 – 2 cm of powder, and the third layer was 0.5 – 2 cm of crust.

Figure 6 shows Cl^- concentrations measured in snow. Values are between 6 – 173 ng $g^{-1}$with a mean of 38.2 ng g^{-1}. This is slightly higher than the Dibb campaign measurements which had a mean of 27.4 ± 8.9 ng g^{-1}. There appears to be a slight increase in Cl^- concentrations over the course of the summer, probably due to increased transport of sea salt over the ice sheet.

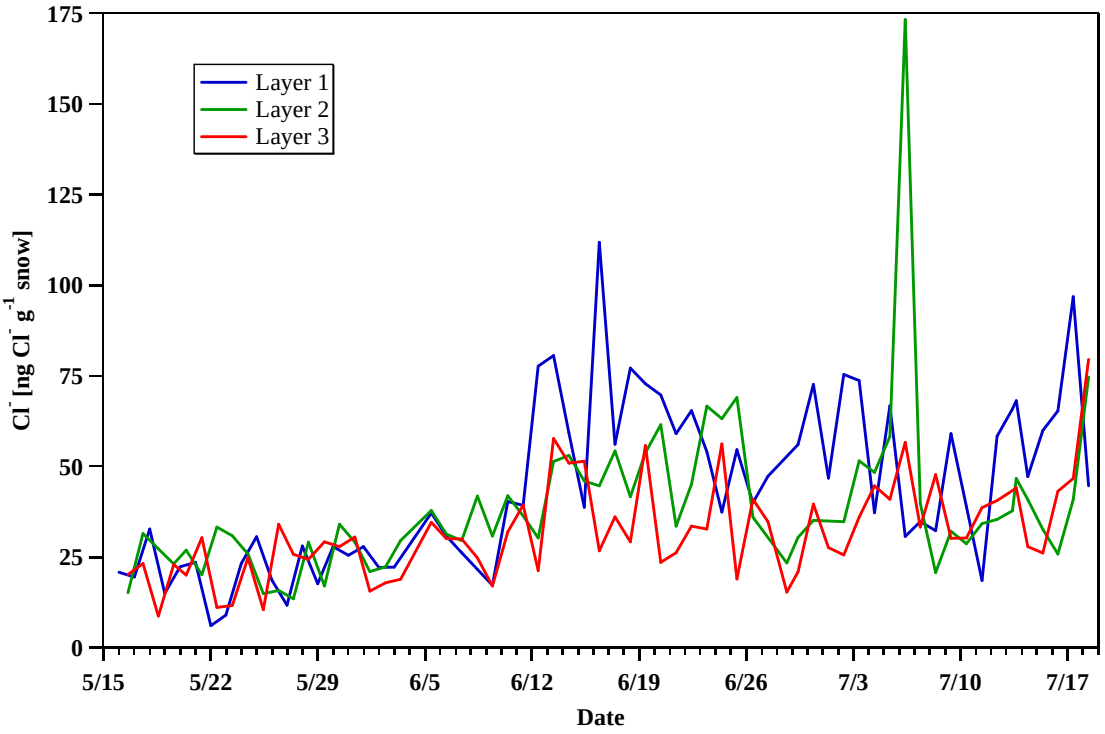

Figure 6: Cl^- concentrations in snow. Typically, the first layer was a few millimeters of newly deposited snow or rime, the second layer was 0.5 – 2 cm of powder, and the third layer was 0.5 – 2 cm of crust.

Figure 7 shows K^+ concentrations measured in snow. Values are between 0.3 – 23 ng g^{-1} with a mean of 3.8 ng g^{-1}. This agrees well with the Dibb campaign measurements which had a mean of 3.4 ± 2.6 ng g^{-1}. There is an increase in K^+ concentrations over the course of the summer, with a peak in mid-June, perhaps due increased emissions from biomass burning. Late summer forest fires could be impacting the K^+ concentrations.

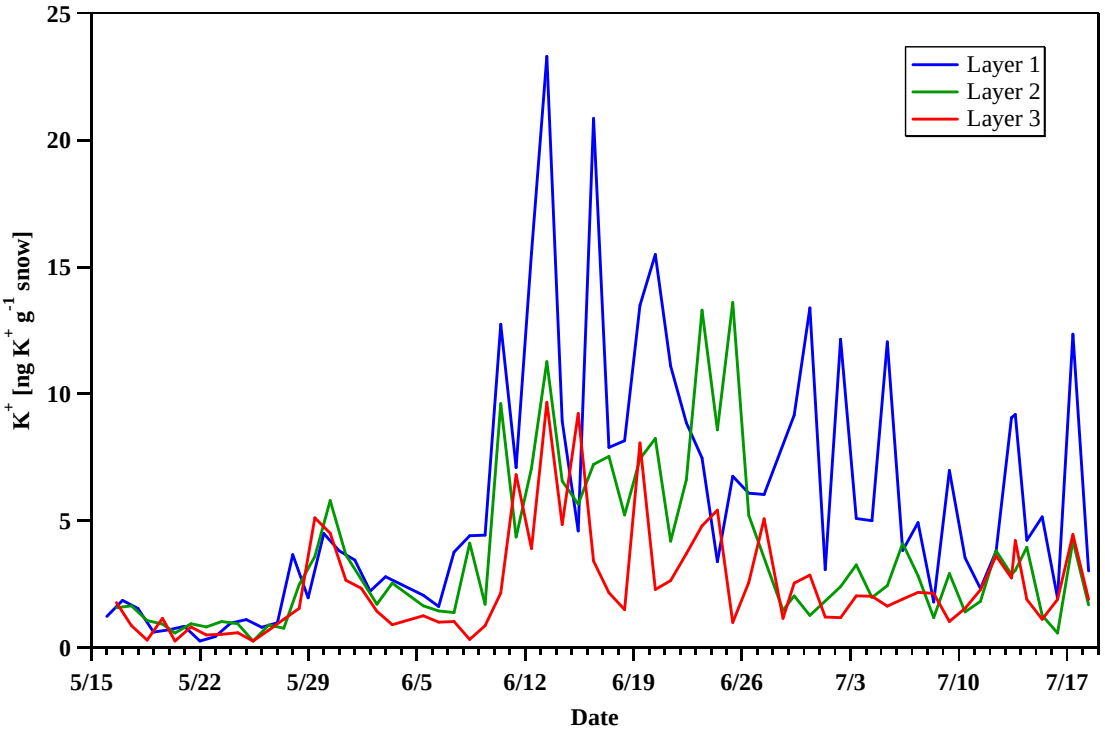

Figure 7: K^+ concentrations in snow. Typically, the first layer was a few millimeters of newly deposited snow or rime, the second layer was 0.5 – 2 cm of powder, and the third layer was 0.5 – 2 cm of crust.

Figure 8 shows NH_4^+ concentration measured in snow. Values are between 0.1 – 38 ng g^{-1} with a mean of 9.5 ng g^{-1}. This agrees well with the Dibb campaign measurements which had a mean of 12 ± 6.9 ng g^{-1}. There is no discernible pattern in NH_4^+ concentrations over the course of the summer.

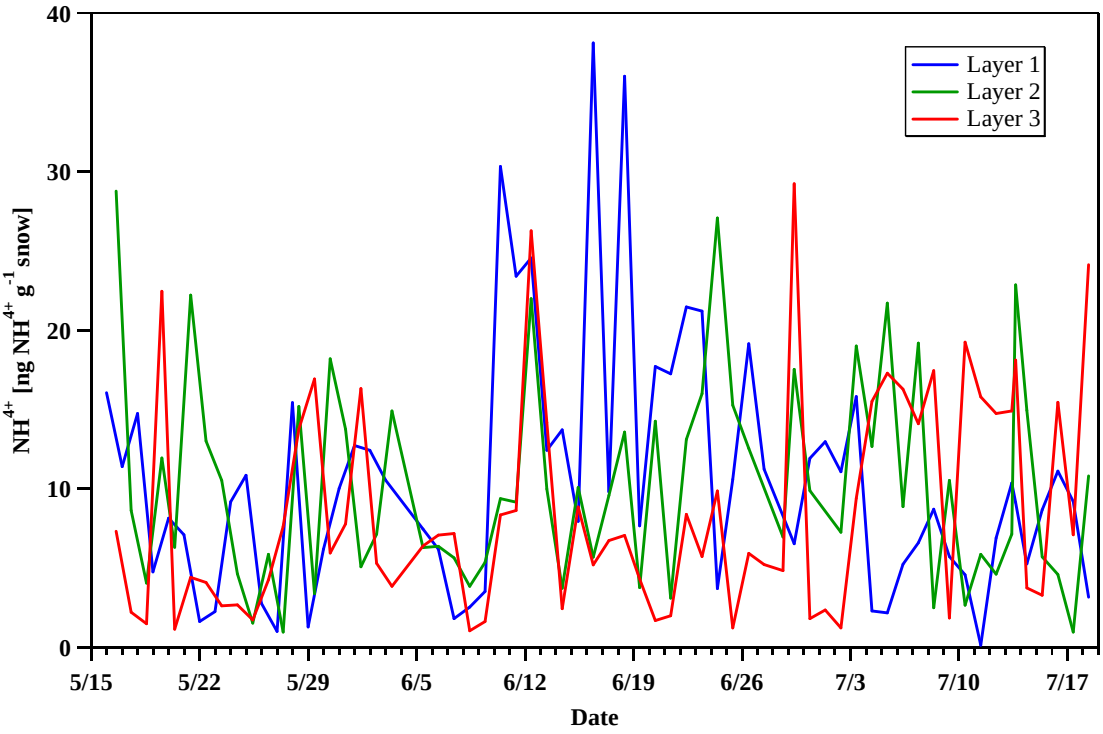

Figure 8: NH_4^+ concentrations in snow. Typically, the first layer was a few millimeters of newly deposited snow or rime, the second layer was 0.5 – 2 cm of powder, and the third layer was 0.5 – 2 cm of crust.

Figure 9 shows NO_3^- concentration measured in snow. Values are between 43 – 650 ng g^{-1} with a mean of 228 ng g^{-1}. This agrees well with the Dibb campaign measurements which had a mean of 216 ± 101 ng g^{-1}. There is no discernible pattern in NO_3^- concentration over the course of the summer. Previous studies have observed broad summer peaks of NO_3^- at Summit [*Dibb et al.*, 2007]. The mid-summer peaks may be due to changing sources or transport.

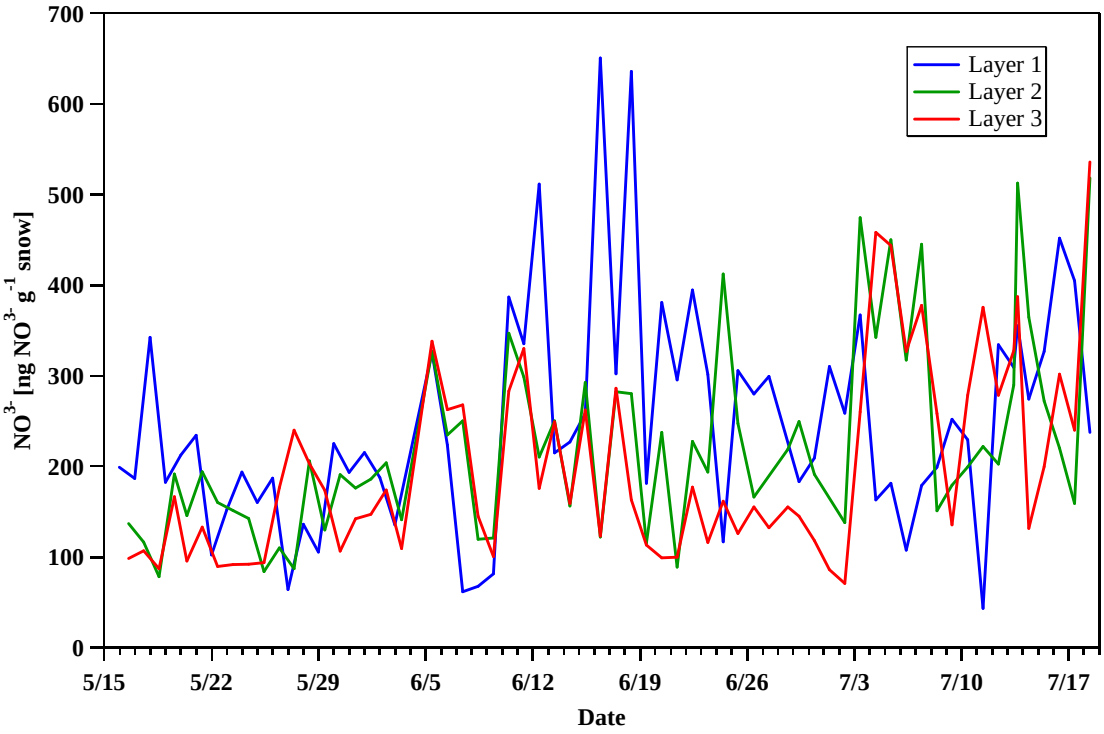

Figure 9: NO_3^- concentrations in snow. Typically, the first layer was a few millimeters of newly deposited snow or rime, the second layer was 0.5 – 2 cm of powder, and the third layer was 0.5 – 2 cm of crust.

Figure 10 shows SO_4^{2-} concentrations measured in snow. Values are between 18 – 225 ng $g^{-1}$with a mean of 100 ng g^{-1}. This is slightly higher than the Dibb campaign measurements which had a mean of 74.7 ± 36.1 ng g^{-1}. There is no discernible pattern in SO_4^{2-} concentration over the course of the summer. Other studies have found that SO_4^{2-} peaks overlapped with dust and/or sea salt peaks [*Dibb et al.*, 2007].

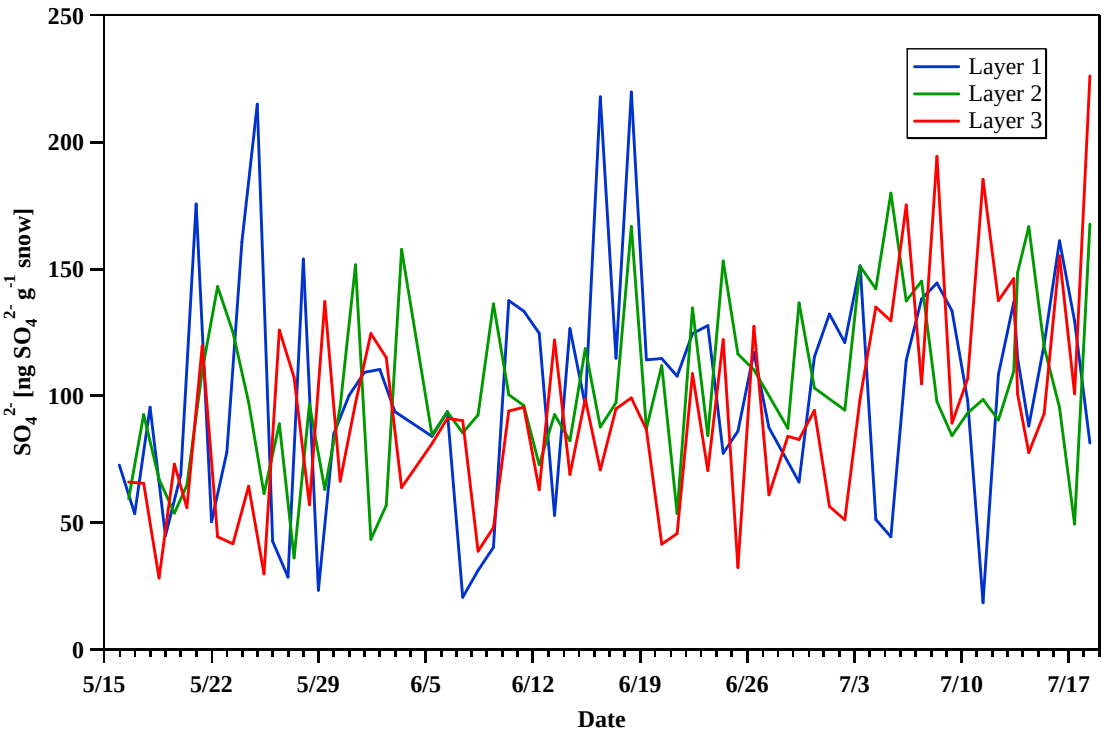

Figure 10: SO_4^{2-} concentrations in snow. Typically, the first layer was a few millimeters of newly deposited snow or rime, the second layer was 0.5 – 2 cm of powder, and the third layer was 0.5 – 2 cm of crust.

Figure 11 shows the concentrations of Al, Na, S, and K in snow. These elements are tracers for dust, sea spray, coal combustion, and biomass burning, respectively. Values for Al are between 0.8 – 205.8 ng $g^{-1}$with a mean value of 19.5 ng g^{-1}. Values for Na are between 0.9 – 67.1 ng g^{-1} with a mean of ng g^{-1}. Values for S are between 17.6 – 64.1 ng $g^{-1}$with a mean of 37.8 ng g^{-1}. Values for K are between 0.8 – 14.4 ng g^{-1} with a mean of 4.9 ng g^{-1}. Previous measurements at Summit showed ranges of 1 – 68 ng g^{-1} for Al [*McConnell*, unpublished results, 2001 - 2011], 1-50 ng g^{-1} for Na, and 0-120 ng g^{-1} for S [*Banta*, 2008]. These agree reasonably well with our measurements. No data for previous measurements of K could be found in the literature.

At least two events are noticeable in the plot with the first and largest event occurring on May 27, 2011, and the second, smaller event occurring May 29, 2011. These events are marked by elevated levels of Al, Na, and K, but not S. It is also possible that the two spikes are not unrelated events but a single event which we sampled twice through error.

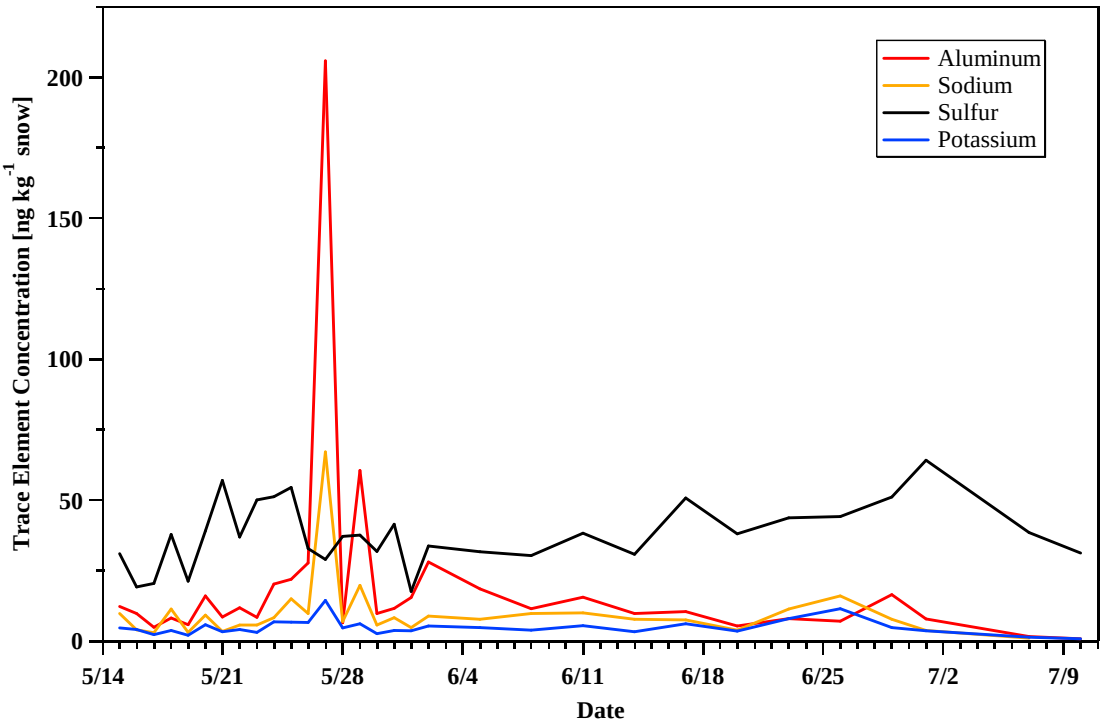

Figure 11: Key element concentrations in snow. Typically, the first layer was a few millimeters of newly deposited snow or rime, the second layer was 0.5 – 2 cm of powder, and the third layer was 0.5 – 2 cm of crust.

Figure 12 and Figure 13 show the mass concentrations of ions, dust, OC, and EC. The vast majority of mass is from ions and dust. Most of the season, ions represent a

larger fraction than dust. The very large dust spike on May 27 appears to be an actual event, but its exact source cannot be determined without further back-trajectory analysis.

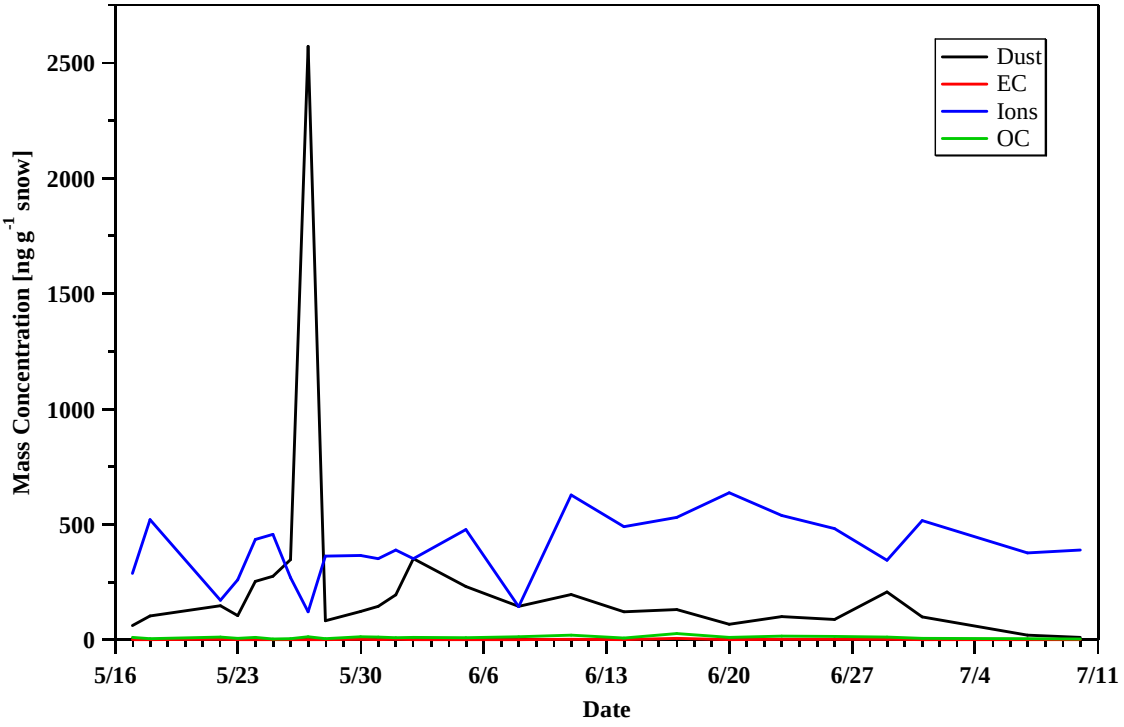

Figure 12: Mass concentrations of ions, dust, OC, and EC.

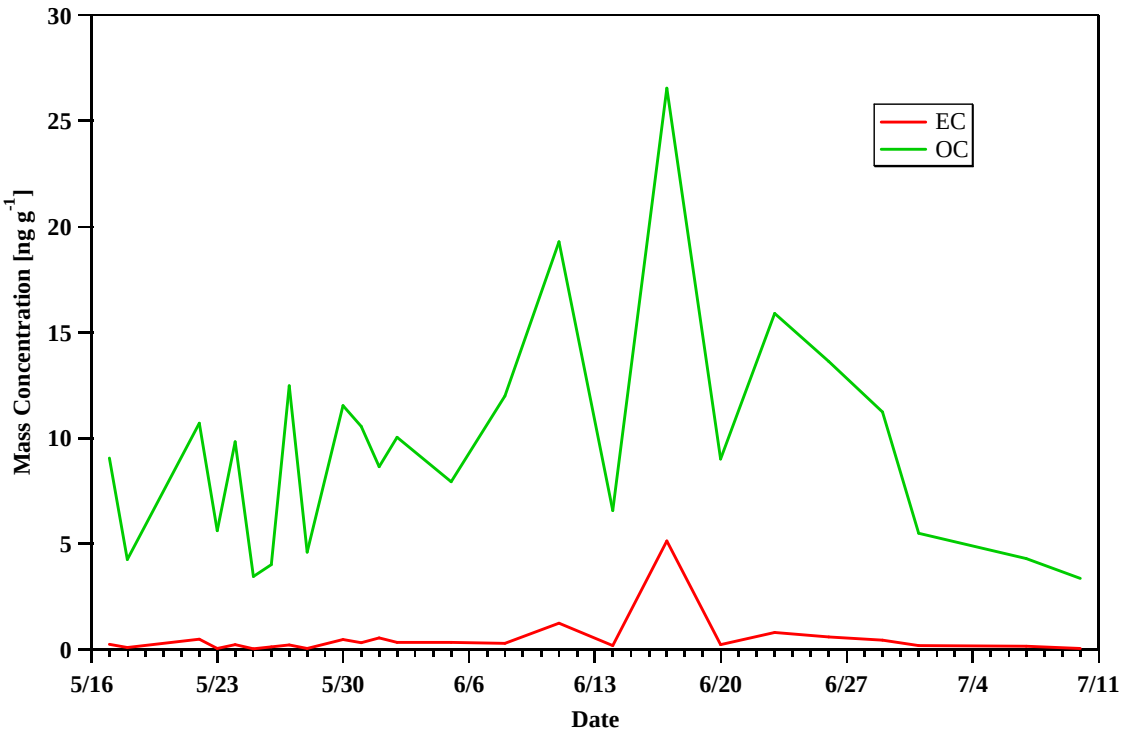

Figure 13: Mass concentrations of EC and OC.

Table 1 presents mass concentration statistics for ions, dust, OC, and EC. The higher mass concentration of dust relative to the other species is due in part to its faster deposition rate to the snow surface [*Bergin et al.*, 1995].

Table 1: Mass concentration statistics for ions, dust, OC, EC, and the dust/EC ratio (computed per day) in snow at Summit.

Quantity	Mean	St Dev	Max	Min	Unit
Ions	395	137	636	120	ng g^{-1}
Dust	246	493	2693	10	ng g^{-1}
OC	9.6	5.4	26.5	3.4	ng g^{-1}
EC	0.51	1.00	5.12	0.03	ng g^{-1}
Dust/EC	1531	2975	12261	25	--

3.2 Real-time Aerosol Measurements

3.2.1 Summer 2011

The plots and figures in this section are all for the period of intensive field sampling between May and July, 2011, although the exact starting dates of each plot vary according to when the instrument was installed.

Table 2 shows statistics for key aerosol properties at Summit in summer 2011. It was not possible to find exact comparisons for each of these quantities at Summit as measurements made at Summit have been scarce. Where it was not possible to compare directly to measurements made at Summit, comparison was made to other Arctic sites.

Previous studies found a summer average σ_{ap} of 0.05 – 0.08 Mm^{-1} for Barrow, Alaska, Zeppelin, Norway, and Alert, Canada, which is significantly lower than our measured mean of 0.14 – 0.15 Mm^{-1} [*Stohl et al.*, 2006]. However, it is thought that Summit is more strongly affected by plumes from mid-latitudes due to the lifting of air masses as explained by the polar dome concept [*Klonecki et al.*, 2003; *Stohl et al.*, 2006]. This may explain the higher values at Summit because the other sites are at or near sea level. A previous study at Summit during summer 2006 found σ_{ap} of 0.15 ± 0.13 Mm^{-1}, which agrees almost exactly with our values [*Hagler et al.*, 2007].

One previous study found an average background AOD of 0.05 with maxima up to 0.55 during extreme plume events at Summit [*Stohl et al.*, 2006]. This average is significantly lower than our value. Measurements by the CIRES sun photometer at Summit during summer 2011 had a value of 0.09 ± 0.04, which agrees very closely with our value of 0.09 ± 0.031 [*Konrad Steffen*, unpublished results, 2011]. This suggests that the previous study may have measured AOD during a summer with lower overall aerosol

loading. Another study at Thule in far northeastern Greenland between 2007 and 2010 found four-year monthly averaged AOD during May, June, and July of 0.09 ± 0.01, 0.055 ± 0.005, and 0.055 ± 0.005, respectively [*Di Biagio et al.*, 2012]. The first of these values agrees well with our measurements, while the values for June and July are on the lower end of our measured AOD.

To the best of our knowledge, previous measurements of angstrom scattering and absorption exponents and aerosol light scattering coefficient have not been made at Summit.

Table 2: Statistics for key aerosol properties at Summit in summer 2011.

Variable	Mean	St Dev	Max	Min	Units
ω	0.93	0.03	0.98	0.87	--
$å_{sp}$	2.08	0.22	2.54	1.10	--
$å_{ap}$	0.73	0.21	1.16	0.24	--
$\sigma_{ap,PSAP}$	0.14	0.12	0.61	0.010	Mm^{-1}
$\sigma_{ap,CLAP}$	0.15	0.13	0.74	0.020	Mm^{-1}
σ_{sp}	1.76	1.23	6.85	0.41	Mm^{-1}
τ_{500}	0.090	0.031	0.21	0.039	--
$å_{AOD}$	1.09	0.28	2.02	0.14	--
$PM_{0.1\text{-}1.0}$	270	180	806	70	$ng\ m^{-3}$

Figure 14 shows aerosol optical depth and coalbedo, defined as 1 – ω. Unfortunately, data is missing for a two-week period from June 1 to June 14 due to a data

collection error. Because of this, it is hard to draw any definite conclusions about the trend in coalbedo over the course of the summer of 2011. AOD peaked in late May and early June of 2011. AOD is presented as the daily average with standard deviation because multiple measurements were taken in each instance.

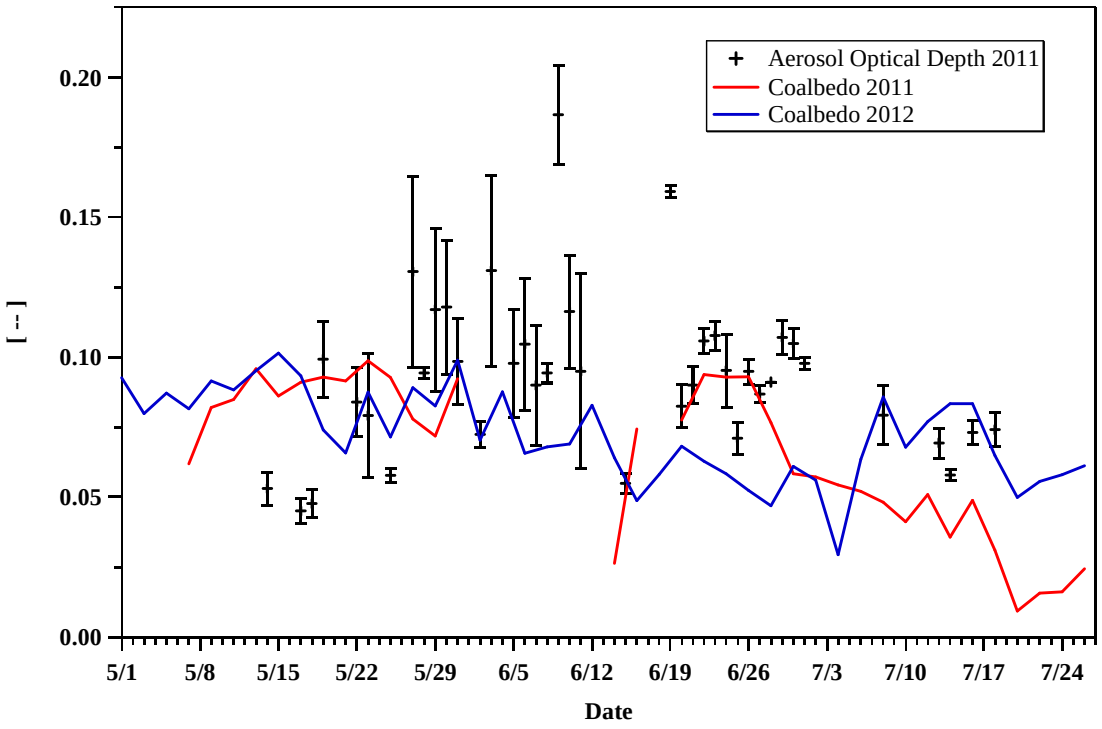

Figure 14: Aerosol optical depth from 2011 and coalbedo (1-ω) from 2011 and 2012 at 550 nm.

Figure 15 shows a timeseries at 550 nm of $å_{ap}$ and $å_{sp}$.

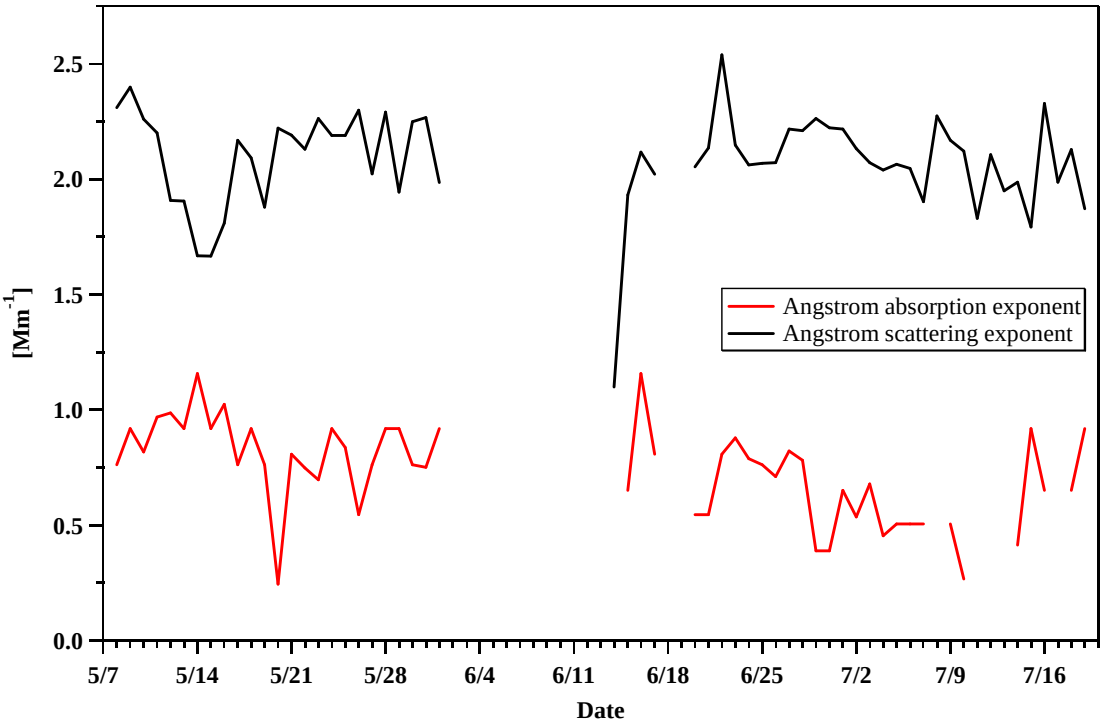

Figure 15: Timeseries of angstrom scattering exponent and angstrom absorption exponent at 550 nm during summer 2011 at Summit.

Figure 16 shows mass concentration of particulate matter between 0.1 µm and 1.0 µm ($PM_{0.1\text{-}1.0}$) over the course of Summer 2011. The mass concentration shows a decline over the course of the summer. This pattern is expected as aerosol loadings are highest in the winter and spring for most locations in the Arctic [*Barrie*, 1986].

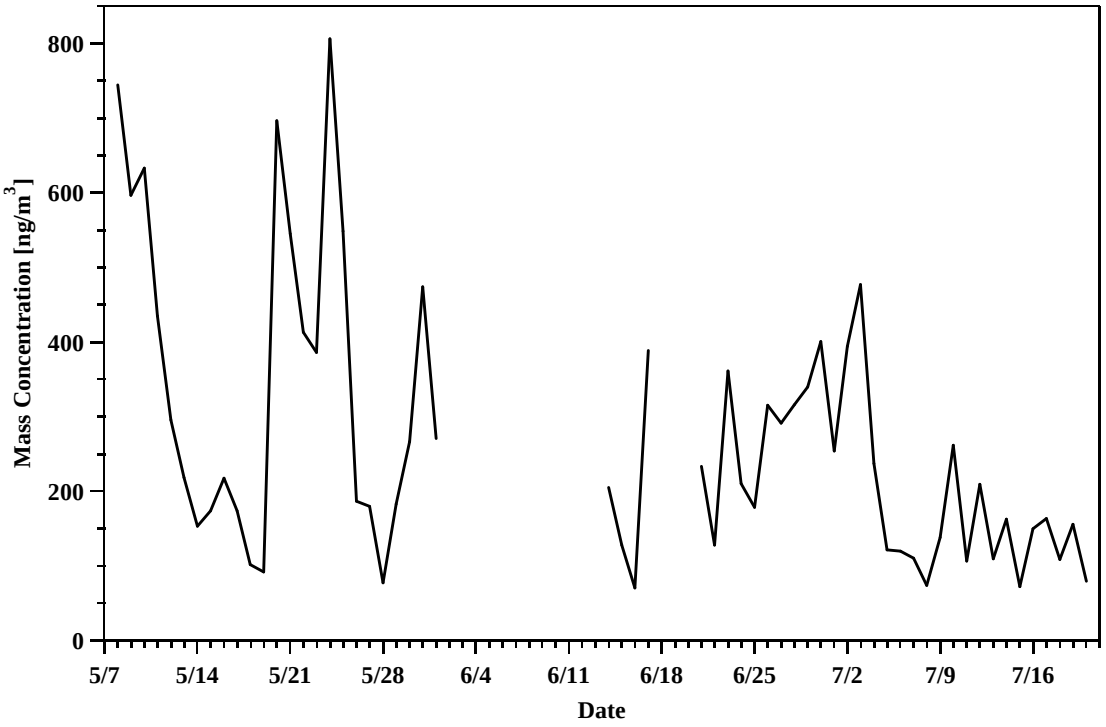

Figure 16: Mass concentration of $PM_{0.1\text{-}1.0}$ over the duration of summer 2011.

Figure 17 through Figure 20 represents the first measurements of CCN that have been made at Summit. Figure 17 and Figure 18 show the raw and clean CCN data, respectively, in a timeseries at five supersaturations. The clean data has had contamination from camp and other sources removed. Contrasting these plots demonstrates that our quality analysis procedures for the real-time data were effective at excluding the contamination plumes from camp. Events in CCN counts are on the scale of 1 – 3 days.

CCN at Barrow have been measured at 20 – 500 cm^{-3} at 1% supersaturation [*Radke et al.*, 1976] in March, while they have been measured on the order of 1000 cm^{-3} over the Arctic Ocean in June [*Saxena and Rathore*, 1984], and also at lower levels of 19.9 – 92.7 cm^{-3} over the Arctic ocean in April 1992 [*Hegg et al.*, 1995]. The

measurements from Summit are on the lower end of this spectrum with a mean of 71 cm^{-3} and a range of 3 – 142 cm^{-3}.

Figure 19 and Figure 20 show the raw and clean CCN data, respectively, plotted as activation fraction versus supersaturation. The activation fraction was calculated as the ratio of the CCN at a given supersaturation versus the CCN at 1% supersaturation. Activation fraction increases as supersaturation increases. This is important for the Arctic because low aerosol number concentrations lead to a higher activation fraction during cloud formation [*Quinn et al.*, 2007].

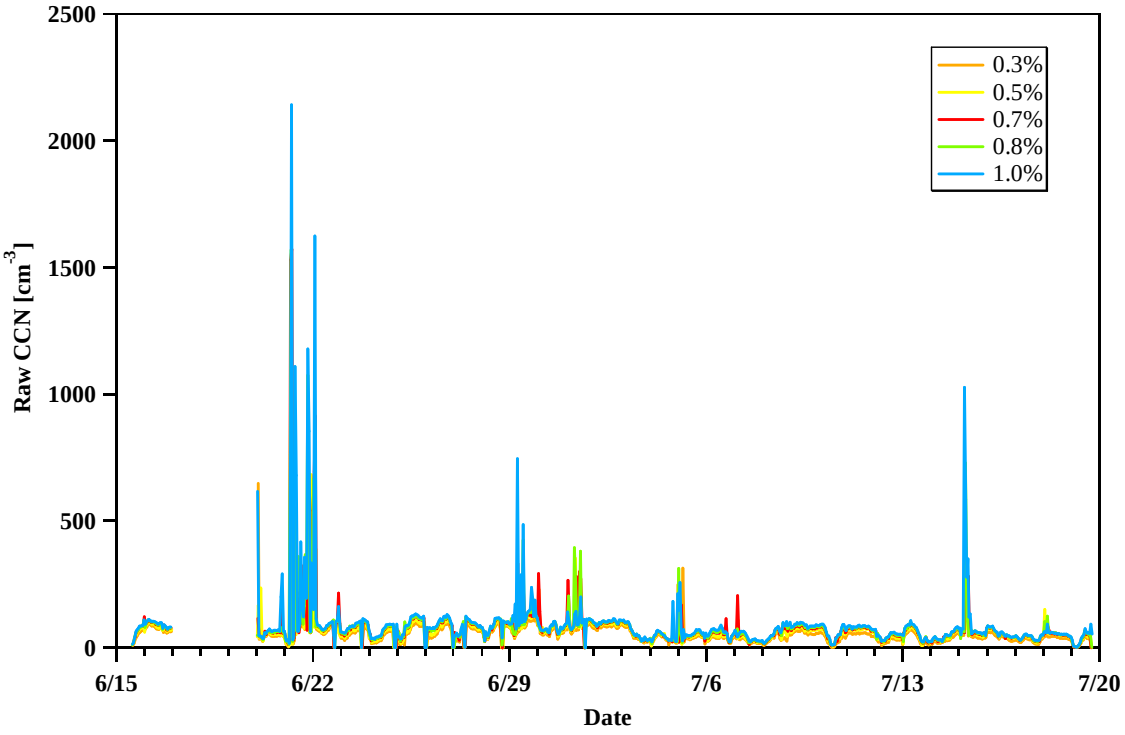

Figure 17: Timeseries of raw CCN data at five supersaturations.

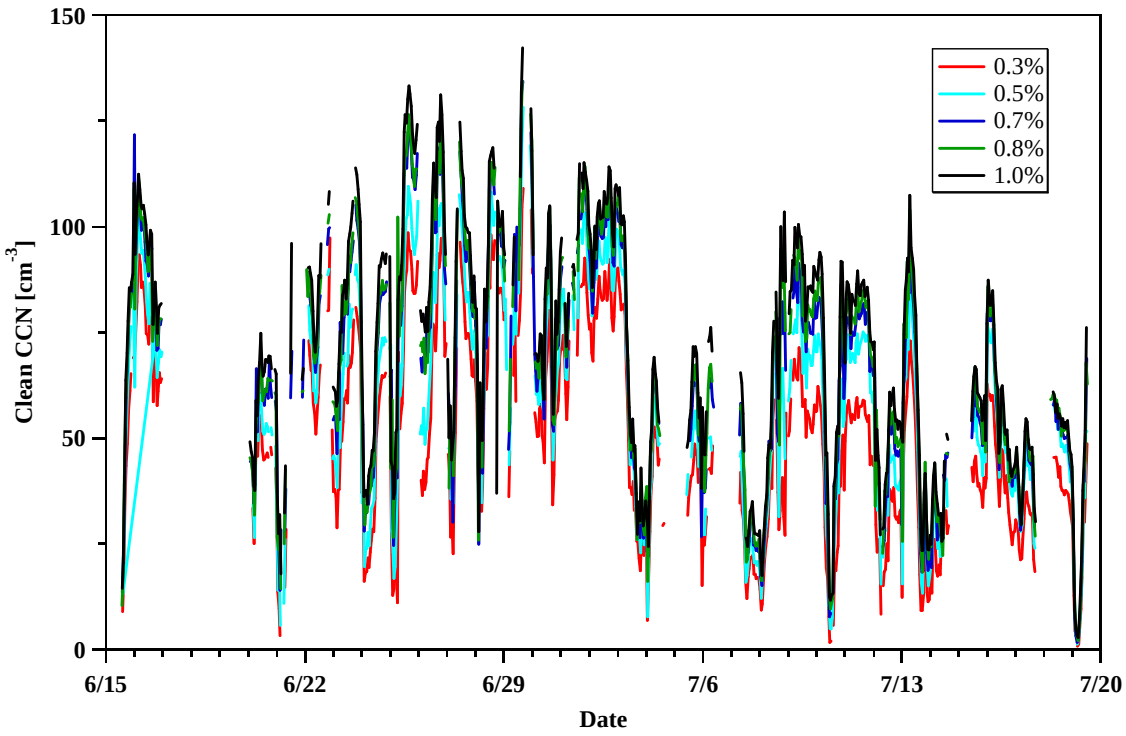

Figure 18: Timeseries of clean CCN data at five supersaturations.

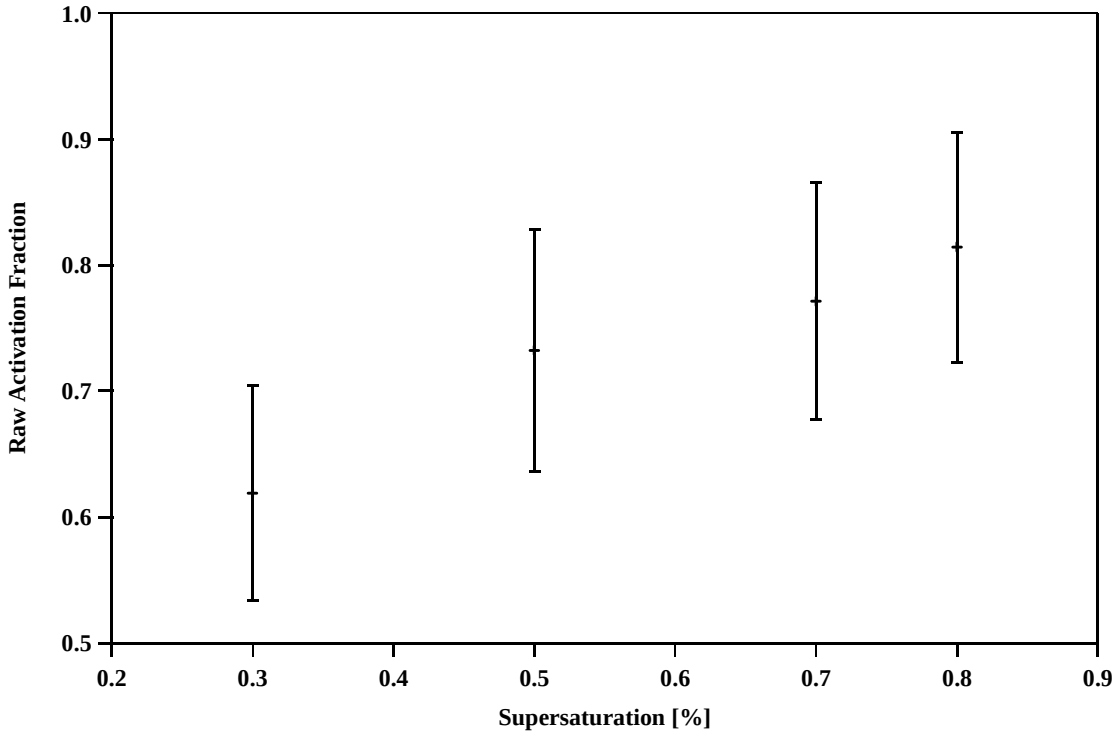

Figure 19: Raw activation fraction versus supersaturation.

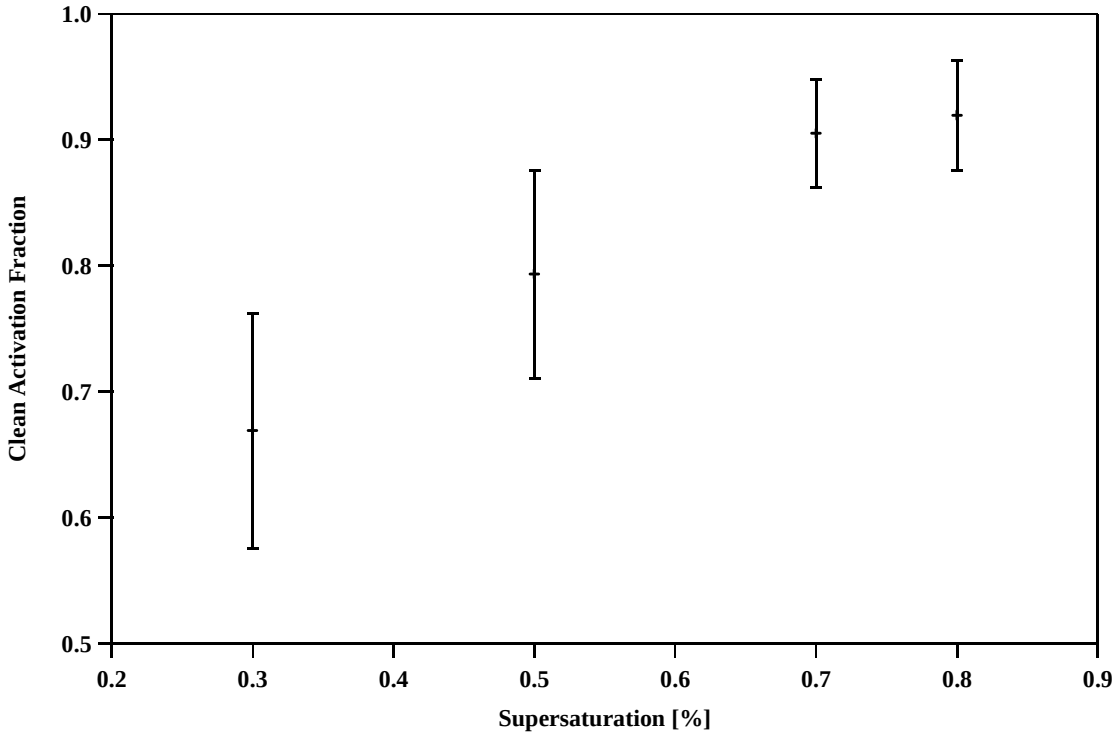

Figure 20: Clean activation fraction versus supersaturation.

Table 3 shows activation fraction statistics at four different levels of supersaturation. It can be seen that the mean activation fraction increases with supersaturation. Above 0.5% supersaturation, more than half of the particles are activated. Activation fraction is calculated as the ratio of CCN to total particles; in this case, the CCN counted at 1% supersaturation was used to approximate total particle count.

Table 3: Activation fraction of CCN at four different levels of supersaturation.

Supersaturation (%)	Activation Fraction			
	Mean	**St. Dev.**	**Max**	**Min**
0.3	0.67	0.09	0.80	0.42
0.5	0.79	0.08	0.92	0.58
0.7	0.91	0.04	0.97	0.78
0.8	0.92	0.04	0.98	0.74

3.2.2 Long-term Measurements

The following plots are for the period May 2011 – Jan 2013. The plots are presented as box plots with the whisker top and bottom representing the 90^{th} and 10^{th} percentile and the box top and bottom representing the 75^{th} and 25^{th} percentile. The plots are based on daily averaged data, which time period was chosen in order to reduce the percentage of data points which were below instrument detection limits. Plots are presented at 550 nm unless otherwise noted.

Figure 21 and Figure 22 show absorption coefficient measured by the PSAP and CLAP, respectively, at 550 nm. The instruments agree well. There is a strong seasonal trend, as it appears that generally σ_{ap} increases through the spring and early summer, decreases in later summer, and then spikes again in the fall before decreasing through the

winter. The mean value of $\sigma_{ap,PSAP}$ is 0.12 ± 0.14 Mm^{-1}. The mean value of $\sigma_{ap,CLAP}$ is 0.09 ± 0.12 Mm^{-1}. Both $\sigma_{ap,PSAP}$ and $\sigma_{ap,CLAP}$ agree well with previous measurements of σ_{ap} made at Summit which found a value of 0.15 ± 0.13 Mm^{-1} [*Hagler et al.*, 2007] using the same PSAP instrument as the one used in this study. Because absorption coefficient is directly proportional to the number of absorbing particles, these measurements suggest that the heaviest absorbing aerosol loading over Summit is during the spring and late summer.

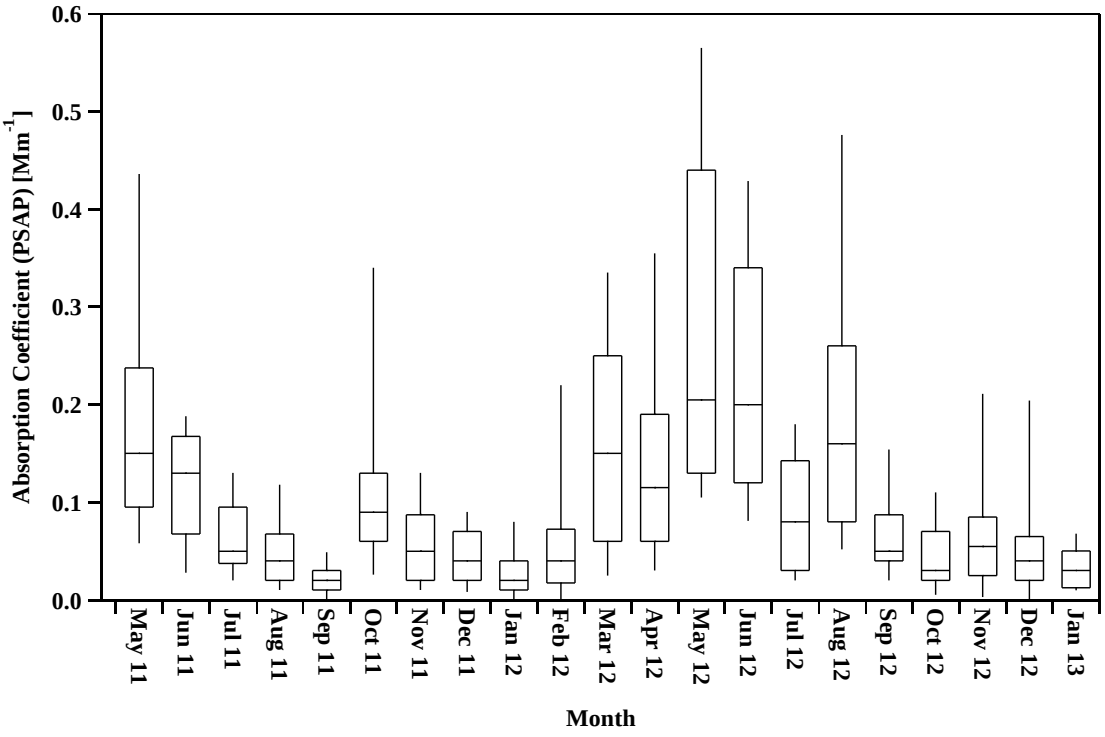

Figure 21: Absorption coefficient (σ_{ap}) measured by the PSAP at 550 nm from May 2011 to January 2013.

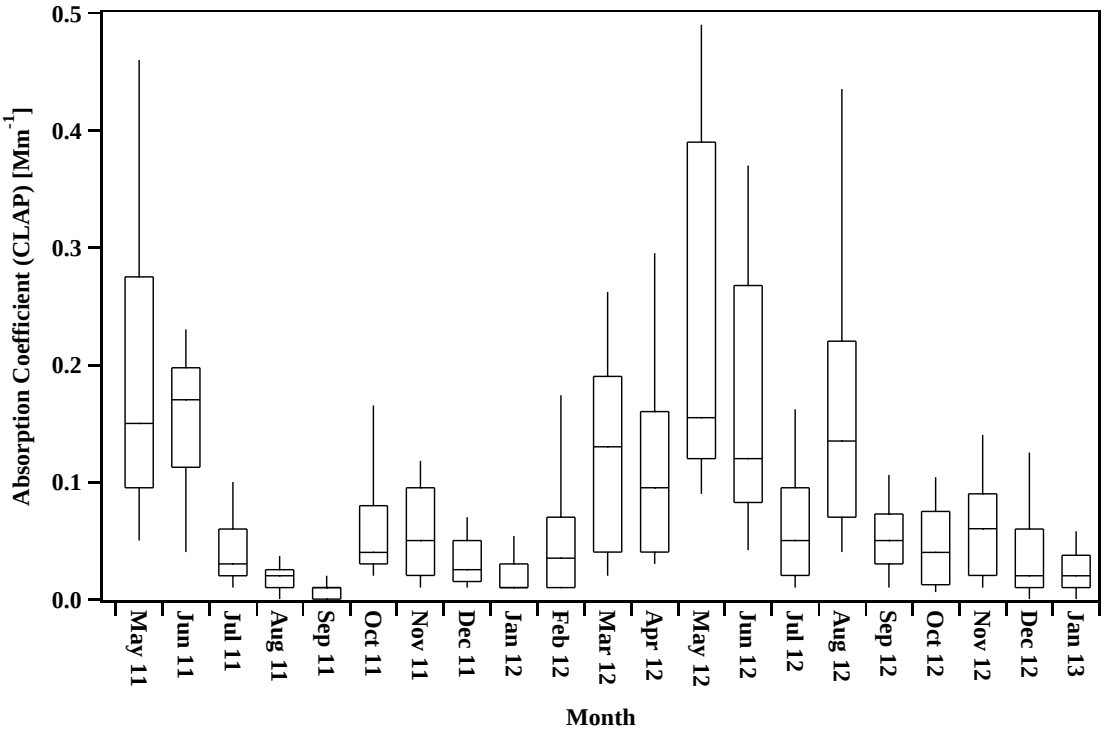

Figure 22: Absorption coefficient (σ_{ap}) measured by the CLAP at 550 nm from May 2011 to January 2013.

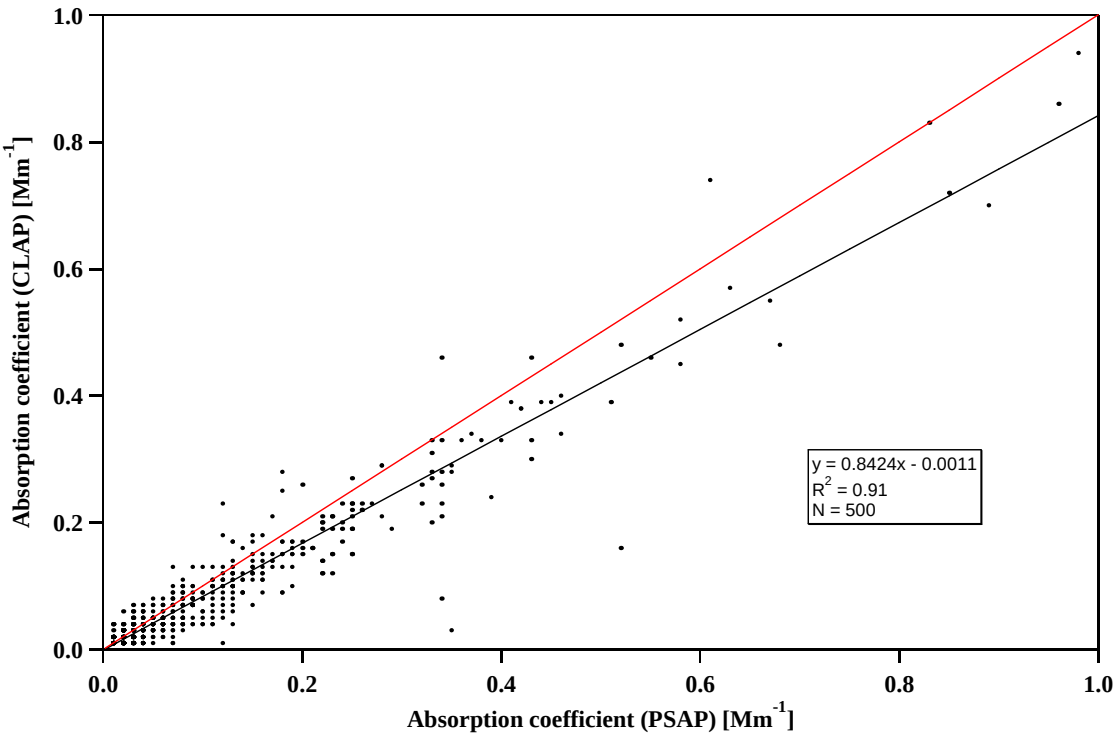

Figure 23: Comparison of CLAP and PSAP absorption coefficients. Red line is 1:1 and black line is linear fit to data.

Figure 23 compares absorption coefficient as measured by the CLAP and PSAP. The two measurements are highly correlated with an R^2 value of 0.91. Although at very large values of σ_{ap} there is more scatter between the PSAP and the CLAP, the vast majority of our measurements fall in the range $\sigma_{ap} < 0.4$ Mm^{-1}, in which range the PSAP and CLAP agree closely.

Figure 24 shows scattering coefficient measured by the nephelometer. There is a strong seasonal trend, as it appears that generally σ_{sp} increases through the spring and early summer, decreases in later summer, and then spikes again in the fall before decreasing through the winter. This is the trend as seen in the absorption coefficient and again implies that aerosol loading is highest in spring and late summer. The high values in August 2012 appear to be the result of several highly scattering events in that time

period. The mean value of σ_{sp} is 1.27 ± 2.08 Mm^{-1}. Since the absorption coefficient and scattering coefficient are proportional to the number of absorbing and scattering molecules per unit volume, respectively, these values indicate that there are more scattering than absorbing particles per unit volume in the aerosol over Summit.

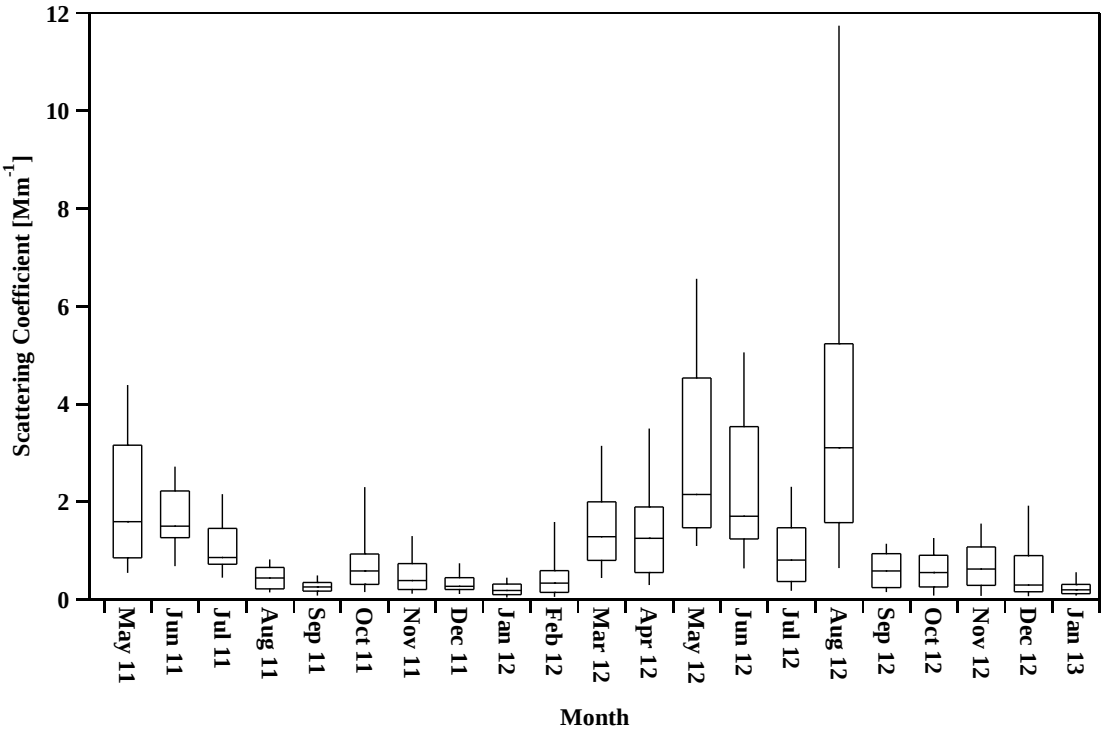

Figure 24: Scattering coefficient (σ_{sp}) at 550 nm from May 2011 to January 2013.

Figure 25 shows the angstrom scattering exponent (450/700 nm). There appears to be a seasonal trend with a smaller range of $å_{sp}$ in May, June, and July. $å_{sp}$ appears to increase in the early summer, decrease slightly as summer progresses, and then experience another rise in late summer/fall before declining in winter. The mean value of $å_{sp}$ is 1.84 ± 0.63. With few exceptions, values of $å_{sp}$ are greater than one, which suggests that the scattering particles are submicron [*Bergin et al.*, 2000].

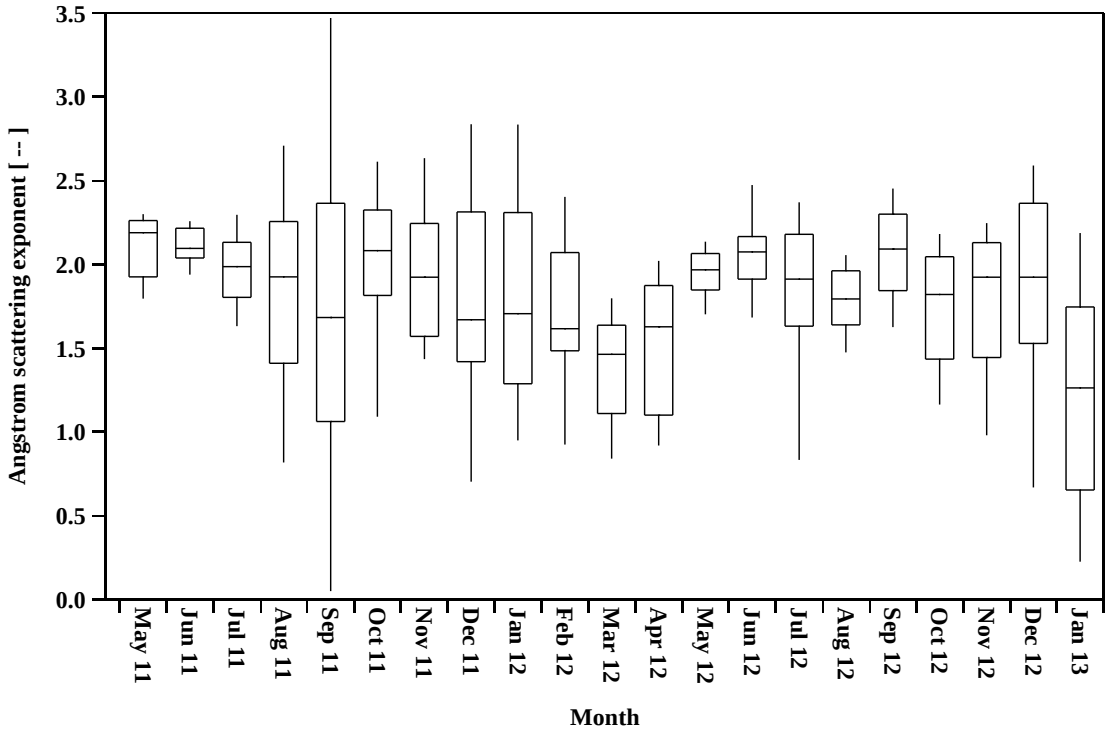

Figure 25: Angstrom scattering exponent (450/700 nm) from May 2011 to January 2013.

Figure 26 shows angstrom absorption exponent (450/700 nm). Besides a very high value in September 2011, the value of $å_{ap}$ remains mostly between 0.7 and 1. The high value and large error bars of September 2011 are due to a scarcity of data in that month as values verged on the instrument detection limit for most of that period. It should be considered cautiously. There is not a strong seasonal trend, although it appears that generally $å_{ap}$ is lower in the spring and late summer/fall and higher in the winter. This is the opposite trend to that displayed by the angstrom scattering exponent. The mean value of $å_{ap}$ is 0.86 ± 0.32.

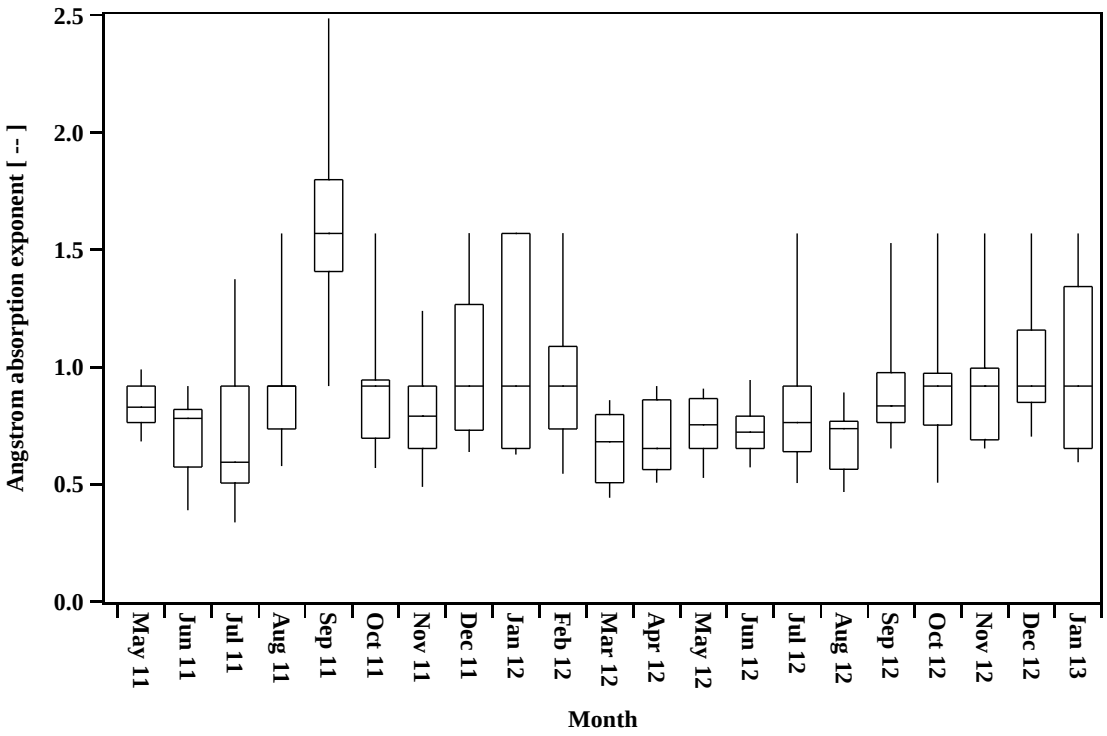

Figure 26: Angstrom absorption exponent (450/700 nm) from May 2011 to January 2013.

Figure 27 shows single scattering albedo. There is a clear seasonal trend, as it appears that generally ω increases through the spring and summer and decreases through the fall and winter. Generally, there is more variability in the single scattering albedo in the winter than in the spring. This may be because total aerosol loading is very low in the winter, so the single scattering albedo responds dramatically to slight changes in the aerosol composition. The mean value of ω is 0.91 ± 0.07. This is a relatively low value for ω considering how remote and pristine Summit is, and it suggests that the aerosol loading over Summit is relatively highly absorbing.

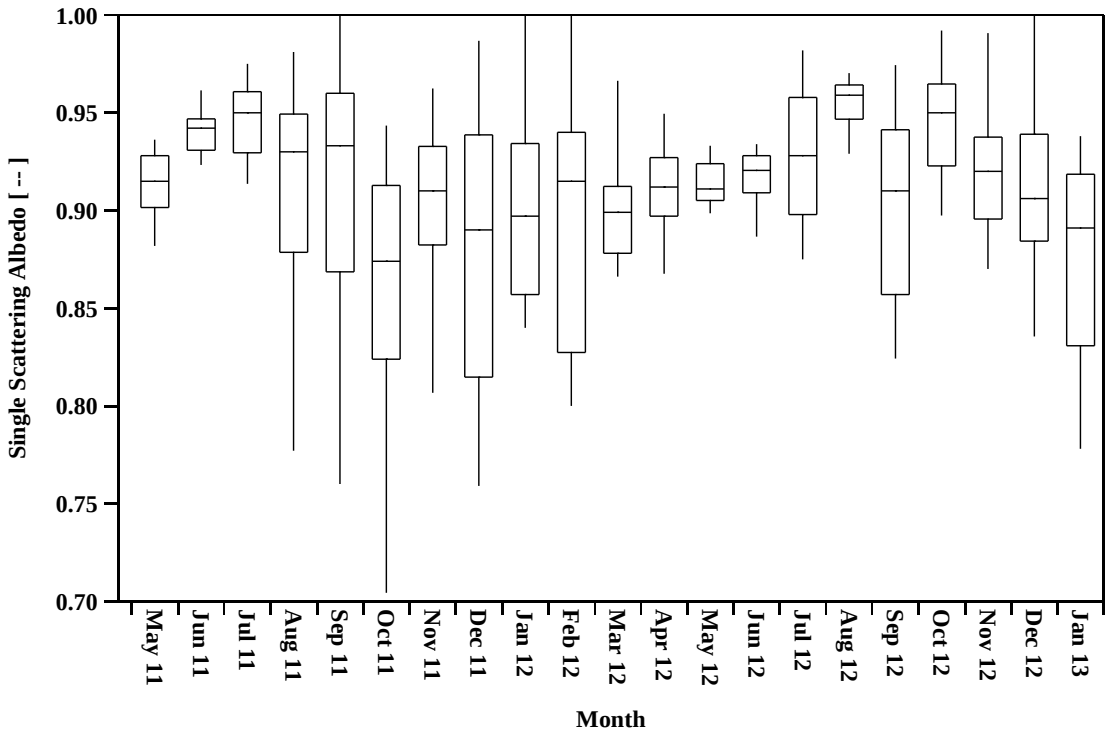

Figure 27: Single scattering albedo at 550 nm (ω_{550}) from May 2011 to January 2013.

Table 4 shows long-term statistics for key aerosol properties measured by the instrument suite.

Table 4: Key aerosol properties measured by the instrument suite.

Quantity	Mean	St Dev	Max	Min	Units
ω	0.91	0.07	1.00	0.50	--
$å_{sp}$	1.84	0.63	5.97	0.16	--
$å_{ap}$	0.86	0.32	2.49	0.24	--
$\sigma_{ap,PSAP}$	0.12	0.14	0.98	0.01	Mm^{-1}
$\sigma_{ap,CLAP}$	0.09	0.12	0.94	0.01	Mm^{-1}
σ_{sp}	1.27	2.08	26.10	0.01	Mm^{-1}

3.3 Clear Sky Direct Aerosol Radiative Forcing Estimates

The data collected in summer 2011 were used to calculate the direct aerosol radiative forcing at the top of the atmosphere (DARF TOA) at Summit using SBDART. To the best of our knowledge, these calculations have never been made for Summit using actual field measurements of the critical aerosol parameters as inputs. The model runs were done for clear sky, high sun conditions, and therefore represent a maximum possible instantaneous DARF. A total of twenty two days were modeled. Table 5 shows statistics for SBDART model results for RFE and DARF TOA, as well as statistics for measured AOD which were included in the modeling study.

RFE presented here is the radiative forcing per unit optical depth at the TOA. The RFE has a value of 127 ± 28 W m^{-2}. The DARF TOA has a value of 11 ± 4 W m^{-2}. There are a limited number of studies to which these estimates of DARF and RFE can be meaningfully compared, principally because Arctic estimates of RFE and DARF over snow-covered surfaces have not been extensively made. However, we include the comparison here in order to illustrate the point that the radiative forcing which we calculated for Summit is relatively large. A modeling study of smoke plumes over Arctic tundra in Barrow, Alaska, found a DARF TOA of 40.8 W m^{-2} for a smoke layer over a snow-covered surface [*Stone et al.*, 2008]. The study assumed a SZA of 65°, broadband surface albedo of 0.80, single scattering albedo of 0.95 at 550 nm, and AOD of 0.72 at 500 nm. Despite the fact that the smoke plume had an AOD nearly eight times greater than the mean value of 0.09 that we measured at Summit, the magnitude of DARF TOA for the smoke plume is only four times the magnitude of DARF TOA which we calculated for Summit. There are two reasons for this: first, the single-scattering albedo

which we measured at Summit is lower than that used for modeling the smoke plume; second, the broadband surface albedo was higher at Summit than that used for the modeling study.

Table 5: Radiative forcing efficiency (modeled), direct aerosol radiative forcing at the top of the atmosphere (modeled), and aerosol optical depth (measured).

Quantity	Mean	St Dev	Max	Min	Unit
RFE	127	28.1	210	82.5	W/m^2
DARF TOA	11.2	3.98	20.9	4.77	W/m^2
AOD (550 nm)	0.088	0.023	0.131	0.045	--

The magnitude of DARF TOA is dependent upon several key variables. We explored this sensitivity with further model runs. Although we lacked the data necessary to do a true seasonal estimate of the DARF TOA and RFE, we conducted model runs for two case study days to explore the effects of single scattering albedo, surface albedo, and SZA on the DARF TOA. May 31 and June 26, 2011, were chosen because they had relatively high single scattering albedos (0.89 and 0.92, respectively). Both days were modeled with an AOD of 0.1. The broadband surface albedo differed between the days with May 31 having a broadband surface albedo of 0.84 and June 26 having a broadband surface albedo of 0.81. For these case study days, standard Arctic parameterizations of atmospheric constituents such as water vapor were applied.

Figure 28 shows a timeseries of the DARF TOA throughout summer 2011. The values shown are for a SZA of 51°. A sensitivity analysis showed that an increase in SZA from 51° to 75° approximately halves the DARF TOA. This represents the change in DARF TOA from high sun to low sun conditions during the summer months at Summit. The decrease in magnitude of DARF TOA as SZA increases is due to reduced direct solar

illumination as the sun gets closer to the horizon. The longer path of the light leads to increased absorption and scattering by intervening particles [*Stone et al.*, 2005].

Figure 29 shows the measured spectral albedo for two case study days. The values agree almost exactly between 350 – 600 nm before gradually deviating. Each day that was modeled in SBDART had a unique spectral albedo profile.

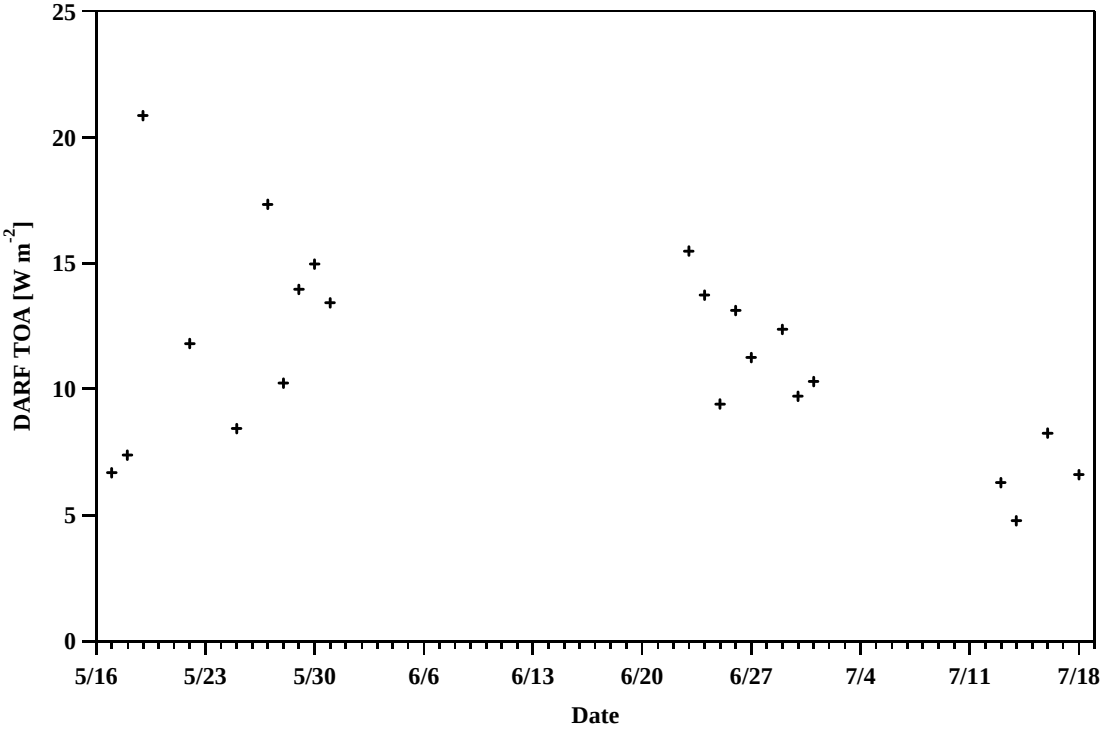

Figure 28: Timeseries of DARF TOA during summer 2011.

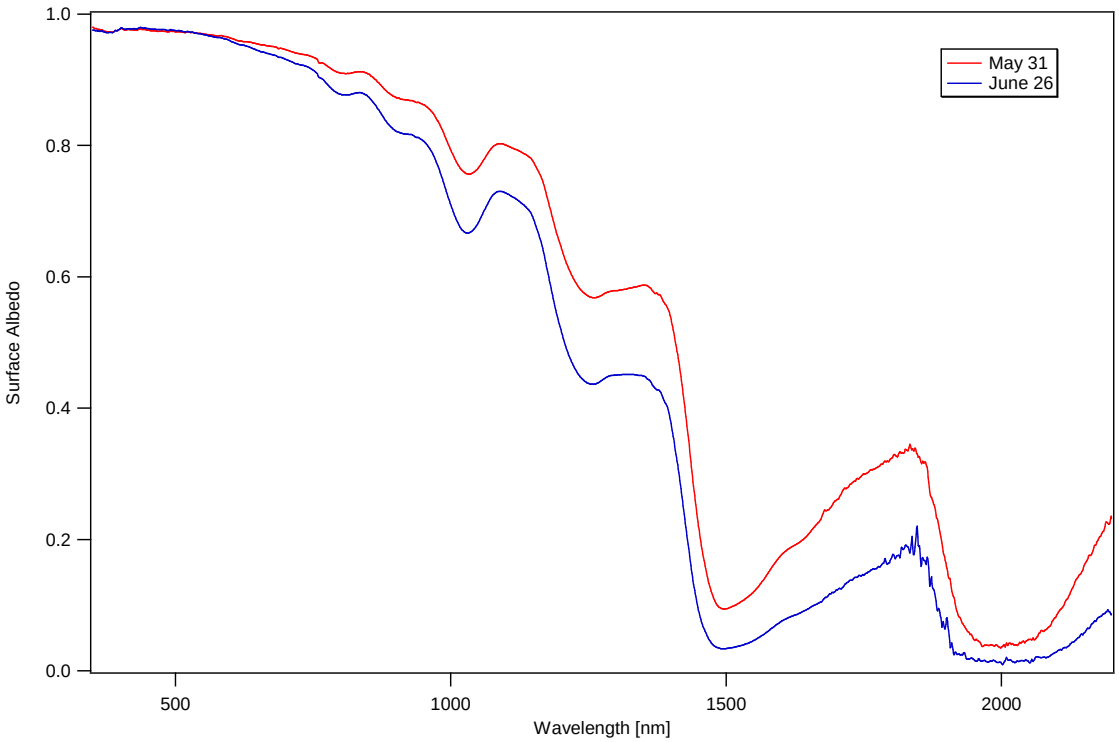

Figure 29: Spectral albedo measured on May 31 and June 26 between 350 and 2200 nm.

Figure 30 shows the effect of single scattering albedo on DARF TOA over the range of single scattering albedo which we would reasonably expect to see at Summit during the summer months. The change in single scattering albedo from highly absorbing ($\omega = 0.87$) to less absorbing ($\omega = 0.95$) approximately halves the DARF TOA for both high and low sun conditions. The reduction of DARF TOA was slightly more than 13 W m^{-2} in high sun conditions and slightly more than 7 W m^{-2} in low sun conditions. These very large shifts in the DARF TOA indicate that the DARF TOA is highly sensitive to changes in the single scattering albedo.

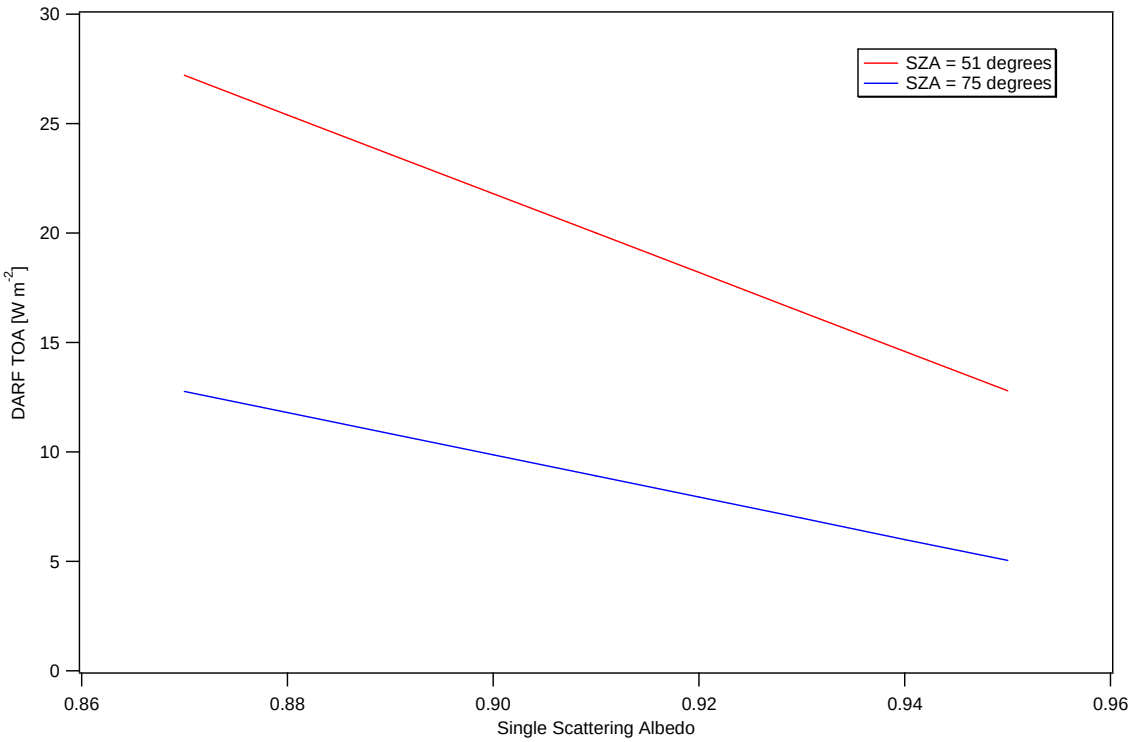

Figure 30: Effect of single scattering albedo on DARF TOA.

The other key factor affecting DARF TOA and RFE is surface albedo. Figure 31 shows the effect of spectral surface albedo on DARF TOA. DARF TOA was calculated over the range of single scattering albedo and at both SZA (51° and 75°) at $R_s = 0.84$ (high albedo) and $R_s = 0.81$ (low albedo). The low albedo DARF TOA was then subtracted from the high albedo DARF TOA to give the difference in forcing between the high and low albedo scenarios. For both high and low sun scenarios, the difference in forcing is less than 1 W m^{-2}, which indicates that the DARF TOA depends far more strongly on single scattering albedo than on spectral surface albedo for the time period during which measurements were made at Summit. Over a surface that experiences seasonal melting the impact of changes in surface albedo would be much more significant, but at Summit the surface temperature is below freezing year-round, so there

is never a decrease in surface albedo due to surface melt. The range of broadband albedo observed during the summer of 2011 was 0.74 to 0.86 [*Wright*, 2012]. Even over this range, the surface albedo impact on DARF TOA would not compare to the effect of the single scattering albedo.

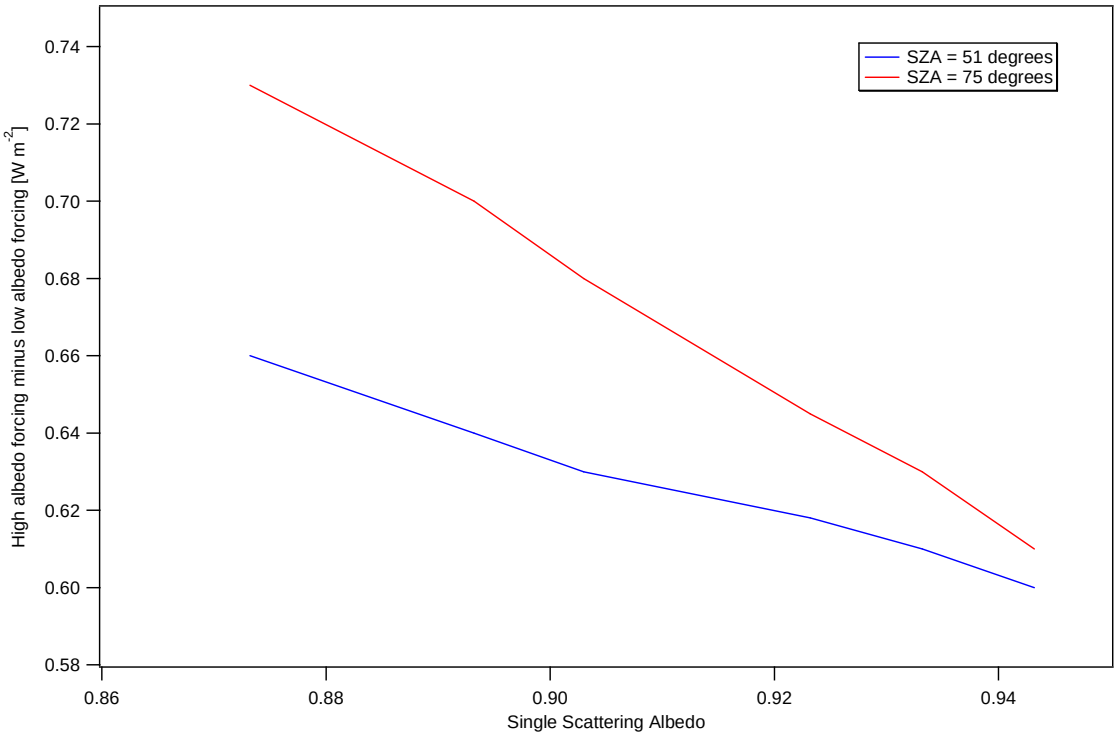

Figure 31: Effect of surface albedo on DARF TOA.

Given these constraints, and also given the fact that it was cloudy approximately half of the summer at Summit in 2011, it is fair to say that the seasonal average DARF TOA for Summit would be significantly lower than the instantaneous forcing presented here. Further measurements, and especially comprehensive measurements of clouds and cloud properties, need to be made in order to quantify the seasonal forcing accurately.

CHAPTER 4

Conclusion

4.1 Summary of Findings

The Greenland ice sheet is subject to much stronger radiative forcing by absorbing aerosols than was previously suspected. This finding has regional and global significance. If these values are representative of the whole of the Greenland ice sheet, which supposition cannot be confirmed at this time due to lack of measurements, it would suggest that warming of the ice sheet may not be accurately modeled in GCMs. Additionally, the very high RFE of absorbing aerosols over the Greenland ice sheet means that it is extremely important to reduce the amount of absorbing aerosols of anthropogenic origin which are transported over Greenland.

A significant outcome of this study was a data set of key aerosol properties for the summer of 2011 and the establishment of a long-term instrument suite at Summit which continuously records key aerosol properties. These measurements have already proven useful in characterizing the aerosol loading and radiative forcing over Summit. The long-term measurements have shown that the aerosol loading over Summit is relatively highly absorbing for a remote, pristine Arctic site. There appears to be a strong seasonal trend with the highest aerosol loadings in early spring and late summer/fall. Background levels of aerosol light scattering and absorption are low, but can be enhanced significantly during events which elevate aerosol loading. Typically, these events last a day to several days.

The study yielded important statistics about aerosol properties at Summit. In summer 2011, the mean value of σ_{sp} was 1.76 ± 1.23 Mm^{-1}; the mean value of σ_{ap} measured by our PSAP was 0.14 ± 0.12 Mm^{-1}, and the mean value of σ_{ap} measured by our CLAP was 0.15 ± 0.13 Mm^{-1}; the mean value of the single scattering albedo calculated with our CLAP was 0.93 ± 0.03; the mean value of $å_{sp}$ was 2.08 ± 0.22; and the mean value of $å_{ap}$ was 0.73 ± 0.21. From May 2011 to January 2013, the mean value of σ_{sp} was 1.27 ± 2.08 Mm^{-1}; the mean value of σ_{ap} measured by our PSAP was 0.12 ± 0.14 Mm^{-1}, and the mean value of σ_{ap} measured by our CLAP was 0.09 ± 0.12 Mm^{-1}; the mean value of the single scattering albedo calculated with our CLAP was 0.91 ± 0.07; the mean value of $å_{sp}$ was 1.84 ± 0.63; and the mean value of $å_{ap}$ was 0.86 ± 0.32.

The study yielded the following conclusions: first, that aerosol loading over Summit shows a clear seasonal trend and is highest in the spring and late summer/fall and lowest in the winter; second, that the clear sky instantaneous direct aerosol radiative forcing at the top of the atmosphere (DARF TOA) has a value of 11.19 ± 3.98 W m^{-2}, which is of much greater magnitude and opposite sign compared to the IPCC estimate of global DARF which has a value of -0.5 (-0.9 to -0.1) W m^{-2}; third, that the radiative forcing efficiency (RFE) of the aerosol over Greenland is very high with a value of 127.38 ± 28.14 W m^{-2}; fourth, that variability in surface albedo (R_s) can alter DARF TOA by approximately 0.25 – 0.5 W m^{-2}; fifth, that variability in single scattering albedo can alter DARF TOA by approximately 5 – 15 W m^{-2}.

4.2 Future Work

Future research in this area must be done in order to further constrain the radiative modeling done in this study. An estimate of seasonal DARF with the inclusion of clouds

is needed. Additionally, more comprehensive air and snow sampling and analysis should be done in order to identity the sources of the absorbing compounds. Furthermore, Greenland is vast, and similar studies need to be performed over much of the ice sheet to fully characterize the regional DARF. As the results of this study indicate that DARF over snow-covered surfaces can have a large magnitude compared to IPCC global estimates, it is important that more estimates of DARF over snow-covered surfaces be made throughout the Arctic.

References

Abdalati, W., and K. Steffen (2001), Greenland Ice Sheet melt extent: 1979–1999, *Journal of Geophysical Research: Atmospheres*, *106*(D24), 33983-33988.

Albrecht, B. A. (1989), Aerosols, cloud microphysics, and fractional cloudiness, *Science (New York, NY)*, *245*(4923), 1227.

Babu, S. S., S. K. Satheesh, and K. K. Moorthy (2002), Aerosol radiative forcing due to enhanced black carbon at an urban site in India, *Geophysical Research Letters*, *29*(18), 1880.

Banta, J. M., Joseph R.; Cahill, Tom; Burkhart, John; Bales, Roger C. (2008), GEOSummit Baseline Measurement Results and Interpretations of Surface Snow Elemental Concentrations, in *NOAA Earth System Research Laboratory Annual Meeting 2008*, edited, Boulder, CO.

Barrie, L. A. (1986), Arctic air pollution: An overview of current knowledge, *Atmospheric Environment (1967)*, *20*(4), 643-663.

Bellouin, N., O. Boucher, J. Haywood, and M. S. Reddy (2005), Global estimate of aerosol direct radiative forcing from satellite measurements, *Nature*, *438*(7071), 1138-1141.

Bergin, M. H., S. E. Schwartz, R. N. Halthore, J. A. Ogren, and D. L. Hlavka (2000), Comparison of aerosol optical depth inferred from surface measurements with that determined by Sun photometry for cloud-free conditions at a continental U.S. site, *Journal of Geophysical Research: Atmospheres*, *105*(D5), 6807-6816.

Bergin, M. H., J. L. Jaffrezo, C. I. Davidson, J. E. Dibb, S. N. Pandis, R. Hillamo, W. Maenhaut, H. D. Kuhns, and T. Makela (1995), The contributions of snow, fog, and dry deposition to the summer flux of anions and cations at Summit, Greenland, *Journal of Geophysical Research: Atmospheres*, *100*(D8), 16275-16288.

Bond, T. C., T. L. Anderson, and D. Campbell (1999), Calibration and Intercomparison of Filter-Based Measurements of Visible Light Absorption by Aerosols, *Aerosol Science and Technology*, *30*(6), 582-600.

Cachier, H., and M. Pertuisot (1994), Particulate carbon in artic ice: Ice archives in Antarctica and Greenland, *Analusis*, *22*(7), M34-M37.

Carmagnola, C., F. Domine, M. Dumont, P. Wright, B. Strellis, M. Bergin, J. Dibb, G. Picard, and S. Morin (2012), Snow spectral albedo at Summit, Greenland: comparison

between in situ measurements and numerical simulations using measured physical and chemical properties of the snowpack, *The Cryosphere Discussions*, *6*, 5119-5167.

Carrico, C. M., M. H. Bergin, J. Xu, K. Baumann, and H. Maring (2003), Urban aerosol radiative properties: Measurements during the 1999 Atlanta Supersite Experiment, *Journal of Geophysical Research: Atmospheres*, *108*(D7), 8422.

Chung, C. E., V. Ramanathan, and D. Decremer (2012), Observationally constrained estimates of carbonaceous aerosol radiative forcing, *Proceedings of the National Academy of Sciences*, *109*(29), 11624-11629.

Church, J. A., and N. J. White (2006), A 20th century acceleration in global sea-level rise, *Geophysical Research Letters*, *33*(1), n/a-n/a.

Chylek, P., and J. Wong (1995), Effect of absorbing aerosols on global radiation budget, *Geophysical research letters*, *22*(8), 929-931.

Chýlek, P., B. Johnson, P. Damiano, K. Taylor, and P. Clement (1995), Biomass burning record and black carbon in the GISP2 ice core, *Geophysical research letters*, *22*(2), 89-92.

Cox, P. M., R. A. Betts, C. D. Jones, S. A. Spall, and I. J. Totterdell (2000), Acceleration of global warming due to carbon-cycle feedbacks in a coupled climate model, *Nature*, *408*(6809), 184-187.

Di Biagio, C., A. di Sarra, P. Eriksen, S. E. Ascanius, G. Muscari, and B. Holben (2012), Effect of surface albedo, water vapour, and atmospheric aerosols on the cloud-free shortwave radiative budget in the Arctic, *Climate Dynamics*, *39*(3-4), 953-969.
Dibb, J. (2013), edited by B. Strellis.

Dibb, J. E., S. I. Whitlow, and M. Arsenault (2007), Seasonal variations in the soluble ion content of snow at Summit. Greenland: Constraints from three years of daily surface snow samples, *Atmospheric Environment*, *41*(24), 5007-5019.

Eckhardt, S., A. Stohl, S. Beirle, N. Spichtinger, P. James, C. Forster, C. Junker, T. Wagner, U. Platt, and S. Jennings (2003), The North Atlantic Oscillation controls air pollution transport to the Arctic, *Atmospheric Chemistry and Physics*, *3*(5), 1769-1778.
Emery, C. A. (1990), One-dimensional modeling study of carbonaceous haze effects on the springtime Arctic environment.

Feng, Y., V. Ramanathan, and V. Kotamarthi (2013), Brown carbon: a significant atmospheric absorber of solar radiation?, *Atmos. Chem. Phys. Discuss*, *13*, 2795-2833.

Frossard, A. A., P. M. Shaw, L. M. Russell, J. H. Kroll, M. R. Canagaratna, D. R. Worsnop, P. K. Quinn, and T. S. Bates (2011), Springtime Arctic haze contributions of

submicron organic particles from European and Asian combustion sources, *Journal of Geophysical Research: Atmospheres*, *116*(D5), n/a-n/a.

Garrett, T. J., L. F. Radke, and P. V. Hobbs (2002), Aerosol effects on cloud emissivity and surface longwave heating in the Arctic, *Journal of the atmospheric sciences*, *59*(3), 769-778.

Goodale, M., and R. Mansfield (1987), Climate Forcing by Anthropogenic Aerosols, *Neuropsychologia*, *25*, 97.

Hagler, G. S., M. H. Bergin, E. A. Smith, J. E. Dibb, C. Anderson, and E. J. Steig (2007), Particulate and water-soluble carbon measured in recent snow at Summit, Greenland, *Geophysical Research Letters*, *34*(16), L16505.

Hagler, G. S. W., M. H. Bergin, E. A. Smith, and J. E. Dibb (2007), A summer time series of particulate carbon in the air and snow at Summit, Greenland, *Journal of Geophysical Research: Atmospheres*, *112*(D21), n/a-n/a.

Hanna, E., P. Huybrechts, K. Steffen, J. Cappelen, R. Huff, C. Shuman, T. Irvine-Fynn, S. Wise, and M. Griffiths (2008), Increased Runoff from Melt from the Greenland Ice Sheet: A Response to Global Warming, *Journal of Climate*, *21*(2), 331-341.

Hansen, J., M. Sato, and R. Ruedy (1997a), Radiative forcing and climate response, *JOURNAL OF GEOPHYSICAL RESEARCH-ALL SERIES-*, *102*, 6831-6864.

Hansen, J., M. Sato, A. Lacis, R. Ruedy, and J. Lelieveld (1997b), The Missing Climate Forcing [and Discussion], *Philosophical Transactions: Biological Sciences*, *352*(1350), 231-240.

Haywood, J., and K. Shine (1995), The effect of anthropogenic sulfate and soot aerosol on the clear sky planetary radiation budget, *Geophysical Research Letters*, *22*, 603-603.

Haywood, J., and O. Boucher (2000), Estimates of the direct and indirect radiative forcing due to tropospheric aerosols: A review, *Reviews of Geophysics*, *38*(4), 513-543.

Hegg, D. A., R. J. Ferek, and P. V. Hobbs (1995), Cloud Condensation Nuclei over the Arctic Ocean in Early Spring, *Journal of Applied Meteorology*, *34*(9), 2076-2082.

Hinds, W. C. (1982), Aerosol technology: properties, behavior, and measurement of airborne particles.

Hobbs, P. V., and A. L. Rangno (1998), Microstructures of low and middle-level clouds over the Beaufort Sea, *Quarterly Journal of the Royal Meteorological Society*, *124*(550), 2035-2071.

IPCC (2007), Climate Change 2007: Synthesis Report, edited, Intergovernmental Panel on Climate Change.

Jacobson, M. Z. (2001), Strong radiative heating due to the mixing state of black carbon in atmospheric aerosols, *Nature*, *409*(6821), 695-697.

Johnson, B. T., K. P. Shine, and P. M. Forster (2004), The semi-direct aerosol effect: Impact of absorbing aerosols on marine stratocumulus, *Quarterly Journal of the Royal Meteorological Society*, *130*(599), 1407-1422.

Karl, T. R., and K. E. Trenberth (2003), Modern Global Climate Change, *Science*, *302*(5651), 1719-1723.

Klonecki, A., P. Hess, L. Emmons, L. Smith, J. Orlando, and D. Blake (2003), Seasonal changes in the transport of pollutants into the Arctic troposphere-model study, *Journal of Geophysical Research: Atmospheres*, *108*(D4), 8367.

Knutson, T. R., J. L. McBride, J. Chan, K. Emanuel, G. Holland, C. Landsea, I. Held, J. P. Kossin, A. K. Srivastava, and M. Sugi (2010), Tropical cyclones and climate change, *Nature Geosci*, *3*(3), 157-163.

Konrad Steffen, S. N. (2011), CIRES Sun Photometer Measurements from Summit, edited.

Krupnik, I., and D. Jolly (2002), *The Earth Is Faster Now: Indigenous Observations of Arctic Environmental Change. Frontiers in Polar Social Science*, ERIC.

Lashof, D. A., and D. R. Ahuja (1990), Relative contributions of greenhouse gas emissions to global warming, *Nature*, *344*(6266), 529-531.

Lough, G. C., J. J. Schauer, J.-S. Park, M. M. Shafer, J. T. DeMinter, and J. P. Weinstein (2004), Emissions of Metals Associated with Motor Vehicle Roadways, *Environmental Science & Technology*, *39*(3), 826-836.

Matt Shupe, B. C. (2012), Cloud fraction and cloud optical depth estimates, edited, NOAA.

McConnell, J. S., Michael (2001 - 2011), Timeseries of Al, Na, S Measurements at Summit, edited, Desert Research Institute.

McCormick, R. A., and J. H. Ludwig (1967), Climate Modification by Atmospheric Aerosols, *Science*, *156*(3780), 1358-1359.

Mote, T. L. (2007), Greenland surface melt trends 1973–2007: Evidence of a large increase in 2007, *Geophysical Research Letters*, *34*(22), n/a-n/a.

Muller, T., J. Henzing, G. De Leeuw, A. Wiedensohler, A. Alastuey, H. Angelov, M. Bizjak, M. Coen, J. Engstrom, and C. Gruening (2011), Characterization and intercomparison of aerosol absorption photometers: result of two intercomparison workshops, *Atmospheric Measurement Techniques*, *4*(2).

Pueschel, R. F., and S. A. Kinne (1995), Physical and radiative properties of Arctic atmospheric aerosols, *Science of The Total Environment*, *160–161*(0), 811-824.

Quinn, P., G. Shaw, E. Andrews, E. Dutton, T. Ruoho-Airola, and S. Gong (2007), Arctic haze: current trends and knowledge gaps, *Tellus B*, *59*(1), 99-114.

Quinn, P., T. Bates, E. Baum, N. Doubleday, A. Fiore, M. Flanner, A. Fridlind, T. Garrett, D. Koch, and S. Menon (2008), Short-lived pollutants in the Arctic: their climate impact and possible mitigation strategies, *Atmospheric Chemistry and Physics*, *8*(6), 1723-1735.

Quinn, P. K., G. Shaw, E. Andrews, E. G. Dutton, T. Ruoho-Airola, and S. L. Gong (2007), Arctic haze: current trends and knowledge gaps, *Tellus B*, *59*(1), 99-114.

Radke, L. F., P. V. Hobbs, and J. E. Pinnons (1976), Observations of Cloud Condensation Nuclei, Sodium-Containing Particles, Ice Nuclei and the Light-Scattering Coefficient Near Barrow, Alaska, *Journal of Applied Meteorology*, *15*(9), 982-995.

Ramanathan, V., P. J. Crutzen, J. T. Kiehl, and D. Rosenfeld (2001), Aerosols, Climate, and the Hydrological Cycle, *Science*, *294*(5549), 2119-2124.

Ramanathan, V., P. J. Crutzen, J. Lelieveld, A. Mitra, D. Althausen, J. Anderson, M. Andreae, W. Cantrell, G. Cass, and C. Chung (2001), Indian Ocean Experiment: An integrated analysis of the climate forcing and effects of the great Indo-Asian haze, *Collections*.

Revelle, R., and H. E. Suess (1957), Carbon Dioxide Exchange Between Atmosphere and Ocean and the Question of an Increase of Atmospheric CO2 during the Past Decades, *Tellus*, *9*(1), 18-27.

Roberts, G. C., and A. Nenes (2005), A Continuous-Flow Streamwise Thermal-Gradient CCN Chamber for Atmospheric Measurements, *Aerosol Science and Technology*, *39*(3), 206-221.

Romanovsky, V. E., S. L. Smith, and H. H. Christiansen (2010), Permafrost thermal state in the polar Northern Hemisphere during the international polar year 2007–2009: a synthesis, *Permafrost and Periglacial Processes*, *21*(2), 106-116.

Satheesh, S., and V. Ramanathan (2000), Large differences in tropical aerosol forcing at the top of the atmosphere and Earth's surface, *Nature*, *405*(6782), 60-63.

Saxena, V., and R. Rathore (1984), Transport and formation of summertime cloud condensation nuclei over the Arctic Ocean, *1984.*, 292-298.

Schuster, G. L., O. Dubovik, and B. N. Holben (2006), Angstrom exponent and bimodal aerosol size distributions, *Journal of Geophysical Research: Atmospheres*, *111*(D7), D07207.

Seinfeld, J. H. P., Spyros N. (1998), *Atmospheric Chemistry and Physics*, John Wiley & Sons, USA.

Shaw, G. (1981), Eddy diffusion transport of Arctic pollution from the mid-latitudes: a preliminary model, *Atmospheric Environment (1967)*, *15*(8), 1483-1490.

Shindell, D., and G. Faluvegi (2009), Climate response to regional radiative forcing during the twentieth century, *Nature Geoscience*, *2*(4), 294-300.

Sirois, A., and L. A. Barrie (1999), Arctic lower tropospheric aerosol trends and composition at Alert, Canada: 1980–1995, *Journal of Geophysical Research: Atmospheres*, *104*(D9), 11599-11618.

Soden, B. J., R. T. Wetherald, G. L. Stenchikov, and A. Robock (2002), Global Cooling After the Eruption of Mount Pinatubo: A Test of Climate Feedback by Water Vapor, *Science*, *296*(5568), 727-730.

Stohl, A., et al. (2006), Pan-Arctic enhancements of light absorbing aerosol concentrations due to North American boreal forest fires during summer 2004, *Journal of Geophysical Research: Atmospheres*, *111*(D22), D22214.

Stone, R., G. Anderson, E. Andrews, E. Dutton, J. Harris, E. Shettle, and A. Berk (2005), Asian dust signatures at Barrow: observed and simulated. Incursions and impact of Asian dust over Northern Alaska, paper presented at Remote Sensing of Atmospheric Aerosols, 2005. IEEE Workshop on, 5-6 April 2005.

Stone, R. S., G. P. Anderson, E. P. Shettle, E. Andrews, K. Loukachine, E. G. Dutton, C. Schaaf, and M. O. Roman (2008), Radiative impact of boreal smoke in the Arctic: Observed and modeled, *Journal of Geophysical Research: Atmospheres*, *113*(D14), D14S16.

Twomey, S. (1977), The Influence of Pollution on the Shortwave Albedo of Clouds, *Journal of the Atmospheric Sciences*, *34*(7), 1149-1152.

Twomey, S. A., M. Piepgrass, and T. L. Wolfe (1984), An assessment of the impact of pollution on global cloud albedo, *Tellus B*, *36B*(5), 356-366.

Valero, F. J., T. Ackerman, and W. Y. Gore (1989), The effects of the Arctic haze as determined from airborne radiometric measurements during AGASP II, *J Atmos Chem*, *9*(1-3), 225-244.

Vermeer, M., and S. Rahmstorf (2009), Global sea level linked to global temperature, *Proceedings of the National Academy of Sciences*, *106*(51), 21527-21532.

Wang, Q., D. Jacob, J. Fisher, J. Mao, E. Leibensperger, C. Carouge, P. Sager, Y. Kondo, J. Jimenez, and M. Cubison (2011), Sources of carbonaceous aerosols and deposited black carbon in the Arctic in winter-spring: implications for radiative forcing, *Atmospheric Chemistry and Physics*, *11*(23), 12453-12473.

Warneke, C., K. Froyd, J. Brioude, R. Bahreini, C. Brock, J. Cozic, J. De Gouw, D. Fahey, R. Ferrare, and J. Holloway (2010), An important contribution to springtime Arctic aerosol from biomass burning in Russia, *Geophys. Res. Lett*, *37*(5), L01801.

Warren, S. G., and W. J. Wiscombe (1980), A model for the spectral albedo of snow. II: Snow containing atmospheric aerosols, *J. Atmos. Sci*, *37*(12), 2734-2745.

Washington, W. M., and G. A. Meehl (1989), Climate sensitivity due to increased CO2: experiments with a coupled atmosphere and ocean general circulation model, *Climate Dynamics*, *4*(1), 1-38.

Wright, P. J. (2012), Comparison of MODIS Snow Albedo To Field Measurements In Central Greenland, University of Houston.

Xi, X., and I. N. Sokolik (2012), Impact of Asian Dust Aerosol and Surface Albedo on Photosynthetically Active Radiation and Surface Radiative Balance in Dryland Ecosystems, *Advances in Meteorology*, *2012*, 15.

Xu, J., M. H. Bergin, R. Greenwald, and P. B. Russell (2003), Direct aerosol radiative forcing in the Yangtze delta region of China: Observation and model estimation, *Journal of Geophysical Research: Atmospheres*, *108*(D2), 4060.

Young, C., I. Sokolik, and J. Dufek (2012), Regional radiative impact of volcanic aerosol from the 2009 eruption of Mt. Redoubt, *Atmospheric Chemistry and Physics*, *12*(8), 3699-3715.

Yu, H., P. Quinn, M. Chin, and L. Remer Chapter II. In-Situ and Remote Sensing Measurements of Aerosol Properties, Burdens, and Radiative Forcing.